Enabling Recycling of Multi-Material 3D Printed Objects through Computational Design and Disassembly by Dissolution

Xin Wen
ATLAS Institute
University of Colorado Boulder
Boulder, Colorado, USA
xin.wen@colorado.edu

S. Sandra Bae
ATLAS Institute
University of Colorado Boulder
Boulder, Colorado, USA
sandra.bae@colorado.edu

Michael L. Rivera
ATLAS Institute and Department of Computer Science
University of Colorado Boulder
Boulder, Colorado, USA
mrivera@colorado.edu

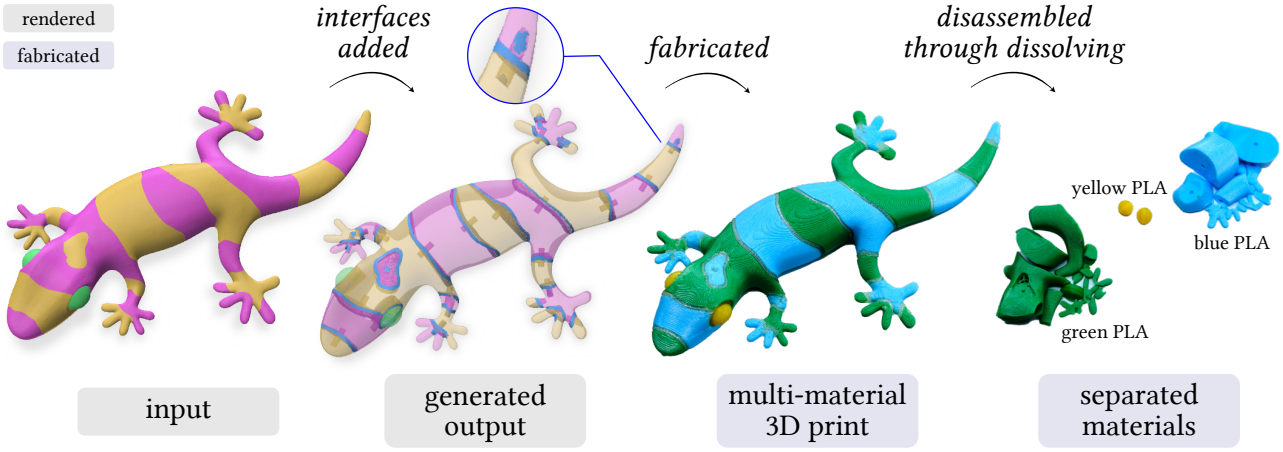

Figure 1: Our computational design technique uses disassembly by dissolution to enable recycling of multi-material 3D printed objects. As an example, dissolvable interfaces are generated in a three-part 3D model of a lizard. Once the object is fabricated, these interfaces can be dissolved, separating the object's individual materials for recycling.

Abstract

Multi-material 3D printing combines the functional properties of different materials (e.g., mechanical, electrical, color) within a single object that is fabricated without manual assembly. However, this presents sustainability challenges as multi-material objects cannot be easily recycled. Because each material has a different processing temperature, considerable effort must be used to separate them for recycling. This paper presents a computational fabrication technique to generate dissolvable interfaces between different materials in a 3D printed object without affecting the object's intended use. When the interfaces are dissolved, the object is disassembled to enable recycling of the individual materials. We describe the computational design of these interfaces alongside experimental evaluations of their strength and water solubility. Finally, we demonstrate our technique across 9 multi-material 3D printed objects of varying structural and functional complexity. Our technique enables us to recycle 89.97% of the total mass of these objects, promoting greater sustainability in 3D printing.

CHI '25, Yokohama, Japan

ACM ISBN 979-8-4007-1394-1/25/04
https://doi.org/10.1145/3706598.3714080

CCS Concepts

• **Human-centered computing** → **Human computer interaction (HCI)**; • **Social and professional topics** → **Sustainability**; • **Applied computing** → **Computer-aided manufacturing**.

Keywords

multi-material 3D printing, sustainability, plastic recycling, computational fabrication

ACM Reference Format:
Xin Wen, S. Sandra Bae, and Michael L. Rivera. 2025. Enabling Recycling of Multi-Material 3D Printed Objects through Computational Design and Disassembly by Dissolution. In *CHI Conference on Human Factors in Computing Systems (CHI '25), April 26–May 01, 2025, Yokohama, Japan.* ACM, New York, NY, USA, 21 pages. https://doi.org/10.1145/3706598.3714080

1 Introduction

Additive manufacturing, or simply 3D printing, has proven useful for fabricating objects with custom functionality across domains such as robotics, electronics, assistive technology, and education [39, 61]. Multi-material 3D printing combines different materials in an object to leverage their unique functional properties (e.g., mechanical, electrical, thermal, color) within a single object that can be fabricated without manual assembly [60]. Until recently, approaches to multi-material 3D printing have required expensive

machines (ranging in cost from 20,000[1] to 300,000[2] USD), or significantly increased fabrication time (e.g., through manual [27] or automated filament switching processes [56, 67]). The advent of more affordable multi-extruder thermoplastic 3D printers—such as the Snapmaker J1[3] (~1000 USD), the Jubilee [89] (~2000 USD), and the Prusa XL[4] (2000-4000 USD)—has opened multi-material 3D printing up to the general public. With access to multi-material 3D printing growing, its environmental impact has become more pressing [1, 20, 23, 77].

On its own, single-material 3D printing with thermoplastics has significant sustainability challenges [23, 24, 69]. However, a single-material object—typically made from a thermoplastic like Polylactic Acid (PLA)—could potentially be recycled in specialized facilities [8, 55, 96] or at home [19]. In contrast, multi-material objects are more challenging, and in some cases impossible, to recycle [20, 23, 52, 55, 77]. Because each material has a different processing temperature, a multi-material object must be disassembled so that its various components can be processed and recycled separately [1, 77]. As a result, a multi-material 3D printed object—for example, made of PLA and flexible thermoplastic polyurethane (TPU)—would generally be considered unrecyclable and end up in a landfill causing detrimental ecological effects like the majority of plastic waste around the world [13, 54].

Challenges with recycling multi-material objects are present in many industries including electronics [83], textiles [21], and construction [65]. Growing concerns over material consumption and a lack of recycling have led these industries to explore Design for Disassembly (DfD) as a possible remedy [33, 44, 87, 90, 93]. DfD is a sustainable practice of designing objects such that they can be disassembled into parts that can be recycled or reused at the object's end of life [10, 86].

This work draws inspiration from DfD approaches to explore how to design and fabricate multi-material 3D printed objects such that they can be disassembled into separate material components for recycling at their end of life. While techniques such as fasteners (e.g., screws, nuts, bolts) could potentially support disassembly, they require significant manual effort to assemble and then later disassemble an object at its end of life [90]. Instead, this work examines computationally designing dissolvable interfaces that are printed between different materials in a 3D printed object, and do not affect the object's intended use. When the interfaces are dissolved, the object is disassembled to enable recycling of the individual materials. Having the ability to recycle these objects can greatly reduce a material's environmental impacts. For example, recycling of PLA and polyethylene terephthalate glycol (PETG) back into 3D printing filaments results in more than a 50% reduction in their respective carbon footprints when compared with new material [42].

This work specifically focuses on dissolvable interfaces printed using Polyvinyl Alcohol (PVA)[5], a commonly used water-soluble support material for 3D printing. However, we note that our computational approach is applicable to other dissolvable 3D printing materials including high-impact polystyrene[6] (HIPS) which is soluble in d-limonene, a renewable material produced from citrus fruits [36].

With this in mind, we present the computational design of these dissolvable interfaces alongside experimental evaluations of their strength and water solubility. Finally, we demonstrate our technique across 9 multi-material 3D printed objects of varying structural and functional complexity. These objects include ones that are flexible, interactive (conductive), and multi-colored. Our results show that this technique can enable the recycling of 89.97% of the total mass of these objects. The remaining mass 10.03% consists of only dissolved material that could also potentially be recycled. We conclude with a discussion of our approach and opportunities to apply it in other manufacturing techniques. Taken together, this work promotes more sustainable outcomes for multi-material 3D printing and digital fabrication as a whole.

2 Related Work

This work builds upon prior efforts in human-computer interaction (HCI), sustainable design and computational fabrication. In this section, we review related work focused on sustainability in digital fabrication, computational design techniques, and dissolvable materials in 3D printing.

2.1 Sustainability in Digital Fabrication

Within the HCI community, there is a growing interest in addressing environmental challenges such as plastic pollution, waste production, and climate change. In particular, research in prototyping and digital fabrication has examined using principles of sustainable design [9, 46] alongside materials that are transient [15], biodegradable [44, 69, 80], and recyclable [12, 69]. Within 3D printing, recent efforts have focused on developing new materials that are bio-based, renewable, and compostable [12, 24, 69]. However, several challenges hinder the adoption of more sustainable materials in 3D printing. These materials generally lack the functional characteristics (e.g., strength) of their thermoplastic counterparts; require custom hardware to be printed; and have print qualities issues due to material shrinkage and warping [12, 24, 69]. With these materials still in their infancy, it is imperative that we find strategies to promote sustainable outcomes with commonly-used 3D printing materials such PLA, PETG, and TPU.

One approach to promote sustainability in 3D printing has been to reduce and reuse printed material. For example, one can insert waste inside of a 3D printed object during fabrication, thereby reducing plastic consumption [92]. However, mixing different materials (e.g., printed vs. non-printed) can lead to monstrous hybrids [52] that either do not readily degrade or are difficult to separate for recycling later. Alternatively, objects can be designed to be assembled and disassembled, for example, by using Lego-like parts [58]. This

[1]Stratasys J55 Full Color: https://www.stratasys.com/en/3d-printers/printer-catalog/polyjet/j55-prime/
[2]Stratasys Objet 350 Connex: https://support.stratasys.com/en/Printers/PolyJet-Legacy/Objet350-500-Connex-1-2-3
[3]Snapmaker J1s: https://us.snapmaker.com/products/snapmaker-j1-independent-dual-extruder-3d-printer
[4]Prusa XL: https://www.prusa3d.com/product/original-prusa-xl-2
[5]Polyvinyl Alcohol (PVA): https://www.simplify3d.com/resources/materials-guide/pva/
[6]HIPS Filament: https://www.simplify3d.com/resources/materials-guide/hips/

can enable parts to be reused, however, it requires significant time and effort to assemble and disassemble objects. It may also alter the intended functionality of an object (e.g., decreasing its strength). We discuss these techniques in more detail in Section 2.2.1.

Recycling 3D printed plastics is a key way to reduce their environmental impacts. Life-cycle assessment has shown recycling 3D printed objects made from PLA and PETG back into printing materials can reduce environmental impacts by 50% [42]. Recyclers of 3D printed plastics are growing—several companies such as TerraCycle [84] and Printerior [66] now accept printed materials when sorted by material type. Single-material objects can be directly recycled. However, multi-material 3D printed objects are difficult to recycle [20, 23]. Their materials need to be processed independently, but cannot be easily separated [1, 77]. Building on principles of design for disassembly [90], we computationally design and fabricate dissolvable interfaces between different materials in 3D printed objects. Once these interfaces are dissolved, the object is disassembled to enable recycling. Crucially, we show that our approach does not alter the object's intended functionality and can promote greater sustainability in 3D printing.

2.2 Computational Design and Multi-Material 3D printing

One of the key advantages of 3D printing over other manufacturing techniques is the ability to directly control the placement of material within an object. Research has explored computational design with this capability to enhance strength [47, 95] and produce desired deformation behavior [2, 51, 53, 75] in 3D printed objects. With multi-material 3D printing, several materials can be combined together to achieve different mechanical properties [64, 91], embed information [49, 94], create sensors [6, 28, 74], and produce color imagery [11, 91]. In this work, we demonstrate our technique across several example multi-material objects that fall into these application domains including a flexible hair brush, an interactive game controller, and multi-color scientific model of a plant cell. Once the interfaces of these objects are dissolved, their various materials (e.g., flexible, conductive, colors) can readily be individually recycled.

2.2.1 Computational Assembly and Disassembly. Computational techniques have also been examined to support the assembly and disassembly of 3D printed objects. For example, automated 3D model segmentation can partition a large object into small printable parts that can be manually assembled after fabrication using glue [14, 38, 48, 88]. Likewise, interlocking joints [81] and velcro-like fasteners [82] can be computationally-generated on objects to enable their manual assembly and disassembly once fabricated. We draw inspiration from these efforts, however, our approach avoids manual assembly and disassembly, which generally makes recycling of multi-material objects far more difficult, if not impossible [20, 52, 77, 90]. Instead, we leverage multi-material 3D printing to produce complete objects that have computationally-generated dissolvable interfaces. Once these interfaces are dissolved, an object is effectively disassembled to enable the recycling of its individual materials.

2.2.2 Multi-Material Attachment Techniques. Our technique relies on dissolvable interfaces being securely attached to other materials. In some cases, the base adhesion strength between two printed materials can be fairly weak. Prior work has examined various techniques such as mechanical interlocking [43, 50, 73] and fastener-like structures (e.g., mushrooms) [78, 82] to increase the attachment strength of two materials in a 3D printed object. In this work, we use similar techniques including interlocking cylindrical and mushroom-shaped structures. As part of our computational approach, these structures are parameterized and can be computationally-generated between a dissolvable interface and another material. In our technical evaluation (Section 4.1), we demonstrate that these structures greatly increase the attachment strength—in some cases, more than the strength of the materials without a dissolvable interface between them.

2.3 Dissolvable Materials in 3D Printing

Dissolvable materials (e.g., water-soluble PVA) are most commonly used in 3D printing as easily removable support structures for objects that have overhanging geometry [34, 40]. Prior work has explored their potential to create transient interactions with 3D printed objects [63]. For example, parts of an object can be printed with temporary labels that assist in the object's assembly and are dissolved afterwards. In addition, parts of a object can dissolved and manually replaced to explore different design iterations [63]. Notably, Hiller and Lipson [35] posited that combining voxel-scale material placement with dissolvable materials could one day be used to disassemble multi-material 3D printed objects for recycling. As a proof-of-concept, they demonstrated a machine that could place small spheres (1.2 mm diameter) made of delrin (a type of plastic) and steel together with a dissolvable glue. Once the glue was dissolved, the spheres could be separated. Building upon this approach, the current work also uses dissolvable materials. However, we present a computational approach that generates dissolvable interfaces between materials of different types in an existing 3D model. In addition, these interfaces can have customizable joints that increase the strength of the adhesion between different materials (discussed more in Section 4). Through this process, our approach preserves the structural and functional qualities of input 3D models, and enables recycling of multi-material 3D printed objects towards the vision of Hiller and Lipson.

3 Computational Design Approach

3.1 Overview

Our computational design algorithm (Figure 2) is implemented in Grasshopper [76], a visual programming language and environment for the 3D modeling program Rhinoceros 3D (Rhino, version 8) [70]. A user imports an existing 3D model as meshes (STLs) that specify different materials or colors (Figure 2, Step 1). Meshes for up to four different materials/colors can be used, assuming the object will be fabricated on a 5-material 3D printer (the fifth material must be dissolvable). The user then adjusts parameters related to the dissolvable interface generation such as the interface thickness ($t_{\text{interface}}$). An overview of user specified interface generation parameters can be found in Table 1.

The algorithm generates a mesh representing the dissolvable interface that is trimmed, or "cut" to fit within bounds of the original input 3D model. It also cuts the interface from the input meshes to fit the interface within. Both the cut interfaces and the cut input

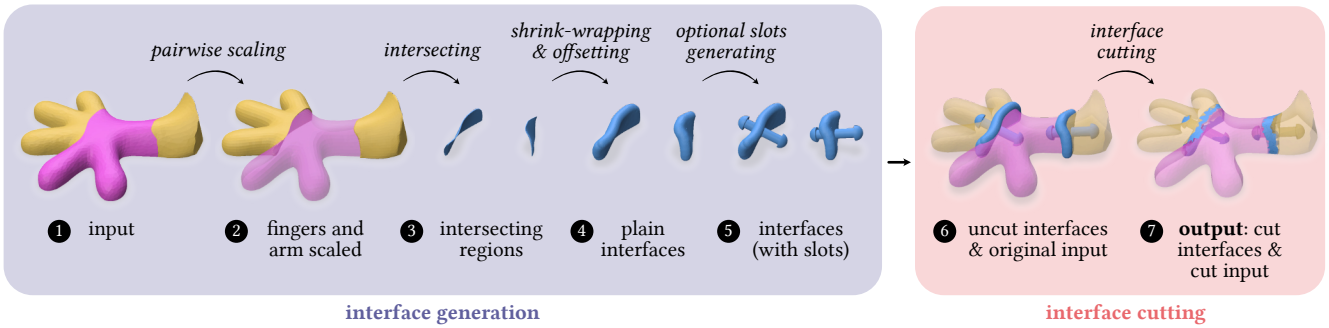

Figure 2: An overview of our computational design approach to generate dissolvable interfaces between different materials in an object for multi-material 3D printing.

meshes are then automatically exported as STL files that can be sliced for multi-material 3D printing using standard slicing software (e.g., PrusaSlicer [68]). The algorithm consists of two main processes: interface generation and interface cutting. Here we describe both of these processes in detail.

3.2 Interface Generation

This process refers to generating the geometry for the dissolvable interfaces between regions where different materials or colors meet in a 3D model. Producing this interface consists of three steps: pairwise scaling and mesh boolean intersection; shrink-wrapping and offsetting; and slot joint generation. For an overview of this algorithm, see Appendix A, Algorithm 1.

3.2.1 Pairwise Scaling and Mesh Boolean Intersection. Creating a dissolvable interface requires knowing specifically where different parts of an input 3D model meet (or "touch"). Typically when a multi-part model is produced in a computer-aided design program, the parts are either cut (segmented) from a solid 3D model, or explicitly designed as separate components whose geometry have faces that touch. In either case, the geometry of these components (i.e., faces and vertices) are often slightly offset from one another and generally do not overlap. Thus, directly using a mesh operation such as boolean intersection to determine where the faces touch is not reliable and will typically not result in complete intersections.

To address this challenge, our algorithm combines pairwise uniform-scaling (Figure 2, Step 2) with mesh boolean intersection (Figure 2, Step 3) to produce the basis of the dissolvable interfaces. Given a list of meshes, M_{input}, our algorithm first reduces the face count of the meshes with a user-defined ratio ρ_{i} to speed up scaling and boolean intersections. The reduced meshes are only used in this step; the original input meshes are used in the later steps for interface cutting to ensure high quality meshes are preserved.

After mesh reduction, our algorithm then applies a user-defined uniform-scale factor, S, to each reduced mesh using its centroid as the scale center to produce a list of scaled meshes, M_{scaled}. Each reduced mesh is then individually boolean intersected with each scaled mesh, excluding the case where the reduced mesh and the scaled mesh correspond to the same input mesh. The resulting intersecting regions are a series of disjoint mesh face groupings (Figure 2, Step 3). To create a dissolvable interface of thickness, $t_{\text{interface}}$, these faces groupings must be converted into closed, offsetable meshes.

3.2.2 Shrink-Wrapping and Offsetting. To produce a closed and offsetable interface meshes, we perform shrink-wrapping [71] in Rhino 8 on each grouping of mesh faces (Figure 2, Step 4). Similar to CGAL's Alpha Wrapping [85], shrink-wrapping works by enclosing an original input geometry in a coarse mesh (much like a convex hull) that is then iteratively carved and refined to approximate the input. The interface thickness, $t_{\text{interface}}$, is used as an input parameter to offset (thicken) the shrink-wrapped interface meshes. As a note, the interface thickness must be at least the minimum extrusion width of the desired 3D printer to ensure it can be fabricated. After offsetting, the resulting interface meshes are "plain" and have no additional adjustments to increase the strength of the bonding between the dissolvable interfaces and other parts for different materials/colors.

3.2.3 Slot Joint Generation. As discussed in Section 2.2.2, attachment between different materials can sometimes be weak, but it can be increased with the addition of mechanical structures (e.g., mushroom-shaped and cylindrical joints). If slot joints, or simply *slots*, are enabled, the algorithm uses parameters for slot type (β: cylindrical or mushroom-shaped), slot height (h_{slot}), and slot radius (r_{slot}) to generate slot joints on all of the shrink-wrapped interface meshes (Figure 2, Step 5). If mushroom-shaped slots are selected, the algorithm also uses the mushroom cap height (h_{cap}) and cap radius (r_{cap}) to generate the mushroom portion (Figure 3, right). We evaluate the mechanical strength of various slot joints in Section 4.1.

To generate slots, our algorithm uses the faces of the shrink-wrapped interface meshes as a base plane. First, it reduces the face count of the shrink-wrapped interface meshes with a ratio ρ_{s}. Reducing the face count helps space potential locations of slot joints and prevent too much overlap once the slots are generated at these locations. The algorithm then selects the closest faces using the distance of each face's centroid to its corresponding interface mesh's centroid. The number of selected faces per interface mesh is based on the number of slot joints per part (κ) desired by the user.

Once the faces are selected, each face's normal vector is used to extrude the slot geometry at the face's centroid (Figure 3, middle). Both cylindrical and mushroom-shaped slots are constructed by

Parameter Name	*Interface Generation Step*	*Purpose*
intersection face reduction ratio, ρ_i	Pairwise Scaling and Mesh Boolean Intersection	The ratio used to reduce the face count of meshes before boolean intersection.
scale factor, S	Pairwise Scaling and Mesh Boolean Intersection	The amount to scale input meshes during pairwise scaling for boolean intersections.
interface thickness, $t_{\text{interface}}$	Shrink-Wrapping and Offsetting	The thickness of the dissolvable interface to generate between two different materials in an object.
interface type, β	Slot Joint Generation	The type of interface to generate—either plain, cylindrical slots, or mushroom slots.
slot count per part, κ	Slot Joint Generation	The number of slots to be generated on each shrink-wrapped part during interface generation.
slot face reduction ratio, ρ_s	Slot Joint Generation	The ratio used to reduce the face count of shrink-wrapped parts to space out slot joints while performing slot generation.
slot height, h_{slot}	Slot Joint Generation	The height of each cylinder generated as a slot joint; for mushroom slots this only defines height of the cylindrical portion.
slot radius, r_{slot}	Slot Joint Generation	The radius of each cylinder generated for a slot joint; for mushroom slots this only defines radius of the cylindrical portion.
mushroom cap height, h_{cap}	Slot Joint Generation	The height of a mushroom cap in mushroom slot joint generation.
mushroom cap radius, r_{cap}	Slot Joint Generation	The radius of a mushroom cap in mushroom slot joint generation.

Table 1: An overview of user-defined interface generation parameters.

extruding a cylinder based on the slot radius, r_{slot}, and slot height, h_{slot} parameters. If bi-directional slot joints are enabled, a cylinder is extruded using both the face's positive and negative normal vectors (Figure 3, right).

For mushroom-shaped slots, the mushroom cap is generated at the top of each cylinder using parameters for the mushroom cap radius, r_{cap}, and cap height, h_{cap}. The algorithm constructs a circular sector using three points: the center point of the top cylinder's circle; a point on a circle with a radius equal to r_{cap} with the same center of the top cylinder's circle; and a point located at h_{cap} distance along the face normal vector away from the center point of the top cylinder's circle. This circular sector is then revolved 360-degrees around the normal vector to form the cap geometry. The cap is then boolean unioned with the cylindrical slot geometry.

Once the slot geometry is generated, the slot meshes are boolean unioned with their corresponding shrink-wrapped interface meshes (Figure 2, Step 5) to create $M_{\text{uncut\_interface}}$, the "uncut" interface meshes. Parameters such as interface thickness ($t_{\text{interface}}$) and slot length (h_{slot}) can result in an initial interface geometry that extends beyond the boundary of the original input model (Figure 2, Step 6).

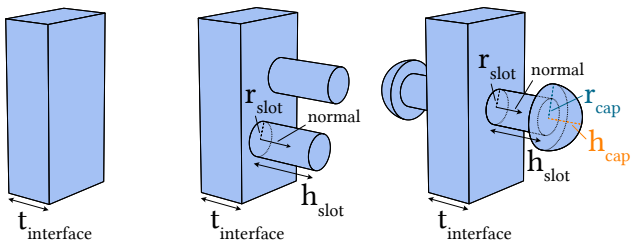

Figure 3: Plain interface (left); cylindrical slots interface (middle); bi-drectional mushroom-shaped slots interface (right).

Because of this, our algorithm must "cut" the interface to remain within the original input geometry as well as subtract the final cut interface geometry from the input models before the meshes can be used for 3D printing.

3.3 Interface Cutting

To ensure that the interface geometry remains within the original input model's geometry, the uncut interface geometry must first be boolean intersected with each original input mesh. Each result of this intersection is then subtracted from the corresponding original input mesh using a boolean difference to produce cut input meshes. At the same time, all of the intersected interface results are unioned to form the cut interface, $M_{\text{cut\_interface}}$. For an overview of this algorithm, see Appendix A, Algorithm 2. The cut interface mesh and all of the cut input meshes are then exported as STL files for 3D printing (Figure 2, Step 7).

Grasshopper's boolean mesh operators attempt to produce solid, closed meshes. When a closed mesh is not possible, it will typically return a null or empty result. The nature of our interface cutting process may result in a mesh that is not closed (e.g., has holes), or has disjoint mesh faces. Thus, we opted to use more robust mesh operators for boolean intersection and difference present in the Libigl geometry processing library [37]. We have written a wrapper library around the Libigl python bindings to interface with the geometry data structures generated from Rhino/Grasshopper. This library allows our entire algorithm to run from within the Grasshopper, or alternatively, the interface cutting procedure can be run using a standalone python script. We visualize the resulting meshes using Polyscope [62].

Once the STL files for the final interface and cut part meshes are generated, they can be input to any slicer software (e.g., Prusa Slicer) for 3D printing.

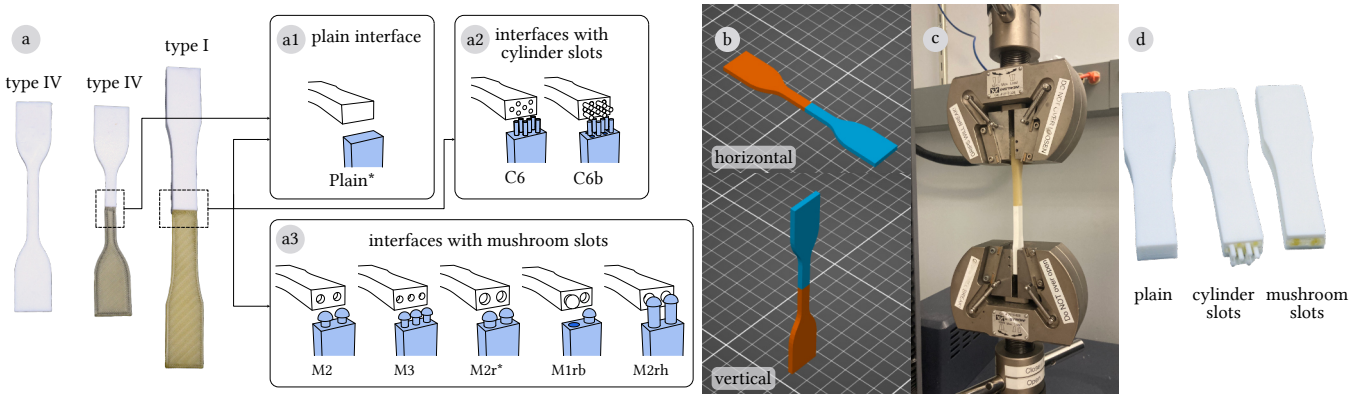

Figure 4: Overview of the tensile strength tests. (a) Example test specimens: Type IV for single material (left), Type IV for dual material with a plain interface (middle), Type I for dual material with a slot interface; Different geometries were tested for dual-material samples with plain interfaces (a1), cylindrical slots interfaces (a2), and mushroom slots interfaces (a3); (b) Two print orientations were used for test samples: horizontal with the tensile load applied parallel to the sample's printed layers (top), and vertical with the tensile load applied perpendicular to the sample's printed layers (bottom); (c) Experimental apparatus for the ASTM standard D638-14 tensile strength test; (d) Example rupture sites for different interface geometries: plain (left), bidirectional cylindrical slots (middle), mushroom-shaped slots (right). The asterisk (*) indicates geometries tested in both print orientations.

4 Technical Evaluation

In this section, we provide technical evaluations of dissolvable interfaces made from PVA. The first evaluation assesses the tensile strength of different interface types when applied to different combinations of 3D printed materials and print orientations. The second evaluation examines the shear strength of different 3D printed materials with different interface types. The last evaluation details the dissolvability of PVA. The results of these evaluations demonstrate the viability of our approach.

4.1 Tensile Strength

To evaluate whether adding PVA interfaces impacts the attachment strength between different materials, we conducted tensile strength tests with two different print orientations according to ASTM standard D638-14 [4]. We also investigated how different types of interface geometries (cylindrical and mushroom-shaped slots) between materials could impact attachment strength. An overview of these tests is shown in Figure 4.

4.1.1 Test Conditions. We tested a variety of samples from commonly used 3D printing filaments—PLA[7], TPU[8], PVA[9], and PETG[10]. We tested several conditions consisting of single-material; dual-material (based on permutations of the four filaments and a white PLA/gray PLA combination) with a "plain" attachment; and various slot joint interface types (cylindrical and mushroom-shaped) using PVA combined with another material. These conditions are summarized in Table 2.

The single-material condition provides a baseline of the tensile strength for the individual materials, and can be validated against widely accepted values [79]. The dual-material condition demonstrates the baseline adhesion strength of two materials plainly interfacing in a typical multi-material object. Lastly, the slot joint interface conditions evaluate whether slot geometry can increase the attachment strength.

For the slot joint interface conditions, we focused on a PLA/PVA material combination to test different types of connections (plain, cylindrical and mushroom-shaped slots). We also explored how the parameters of these connection types impact strength. For cylindrical slots, we examined PVA slots extending into the PLA portion as well as slots in both directions (PVA slots into the PLA half, and PLA slots extending into the PVA half). For mushroom-shaped slots, we examined five variations based on different generation parameters for slot height, stem radius, cap height, and number of slots. Based on the results of the previous conditions, we also tested TPU/PVA with one of the strongest interface types, *M2r*, to further validate that slot interface types can enhance the interface when compared with a plain interface. We chose *M2r* because it both minimizes use of PVA (which is not as readily recyclable as other materials), while supporting similar strength to *M2rh*.

All samples of aforementioned conditions were printed horizontally such that their layers were parallel to the direction that undergoes the tensile load (Figure 4b, top). To test how print orientation affects tensile strength, we conducted additional tests with vertically printed samples, where their layers are printed perpendicular to the direction that undergoes the tensile load (Figure 4b, bottom). In the vertical print orientation, we tested the following conditions: PLA; PVA; TPU; PLA/PVA with plain and *M2r* interfaces; and TPU/PVA with plain and *M2r* interfaces. A summary of the vertical print orientation conditions is shown in Table 3.

[7]Overture PLA: https://overture3d.com/products/overturepla
[8]Overture TPU: https://overture3d.com/products/overture-tpu-filament-1-75mm
[9]Fused Materials PVA: https://fusedmaterials.com/product/fused-materials-pva-3d-filament/
[10]Prusament PETG: https://www.prusa3d.com/product/prusament-petg-prusa-orange-1kg/

Horizontal Print Orientation Tensile Test Conditions				Interface Parameters (mm)			
Material	*Specimen Type*	*Thickness (mm)*	*Interface Geometry*	h_{slot}	r_{slot}	h_{cap}	r_{cap}
PLA	IV	3	N/A	–	–	–	–
PVA	IV	3	N/A	–	–	–	–
TPU	IV	2	N/A	–	–	–	–
PETG	IV	3	N/A	–	–	–	–
White PLA/Gray PLA	IV	3	Plain	–	–	–	–
PLA/PVA	IV	3	Plain	–	–	–	–
TPU/PVA	IV	3	Plain	–	–	–	–
PETG/PVA	IV	3	Plain	–	–	–	–
PLA/TPU	IV	3	Plain	–	–	–	–
PLA/PETG	IV	3	Plain	–	–	–	–
PETG/TPU	IV	3	Plain	–	–	–	–
PLA/PVA	I	7	Plain	–	–	–	–
	I	7	C6	5	0.8	–	–
	I	7	C6b	5	0.8	–	–
	I	7	M2	2.5	1.5	2.5	2.5
	I	7	M3	3	1.2	2	2
	I	7	M2r	2.5	2	2.5	2.5
	I	7	M1rb	2.5	2	2.5	2.5
	I	7	M2rh	7.5	2	2.5	2.5
TPU/PVA	I	7	Plain	–	–	–	–
	I	7	M2r	2.5	2	2.5	2.5

Table 2: Summary of horizontal print orientation tensile test conditions.

Vertical Print Orientation Tensile Test Conditions			
Material	*Specimen Type*	*Thickness (mm)*	*Interface Geometry*
PLA	IV	3	N/A
PVA	IV	3	N/A
TPU	IV	2	N/A
TPU/PLA	I	7	Plain
PLA/PVA	I	7	Plain
	I	7	M2r
TPU/PVA	I	7	Plain
	I	7	M2r

Table 3: Summary of vertical print orientation tensile test conditions.

4.1.2 Sample Preparation. For each condition, we tested five samples (N=5). All samples were sliced in PrusaSlicer with 100% rectilinear infill at 45° angle and a layer height of 0.2 mm. In the single-material condition, we used Type IV specimens printed on a Prusa MK3[11]. In the dual-material condition, we used Type IV specimens printed on a Prusa XL. Lastly, in the slot interface conditions, we used Type I specimens printed on a Prusa XL.

According to ASTM standard D638-14, the sample type should be selected based on the material thickness, material availability, and whether comparison across material classes is required (e.g., rigid vs. flexible). A Type IV specimen is used for materials with a thickness of at most 4 mm, and a Type I specimen is used for materials with a thickness of 7 mm or less. Where thickness was not a factor, we opted to use Type IV specimens to minimize material consumption and support comparison between rigid and flexible materials. All Type IV samples had a thickness of 3 mm except for the TPU samples. We used a 2 mm thickness for the TPU samples because TPU has very high elongation and a 3 mm sample would not break at the test machine's maximum extension. For the slot interface conditions, we used Type I specimens (7 mm thickness) to ensure there would be enough cross-sectional area across the gauge length to incorporate slot joints.

4.1.3 Test Apparatus and Procedure. Tests were performed using an MTS Exceed E43.504 Universal Testing Machine[12] with a 50 kN load cell. All tests except for the pure TPU samples were conducted with a 0.125 mm/s crosshead speed. A 1.00 mm/s crosshead speed was used for the pure TPU samples due to the elasticity of TPU causing significantly longer test runs (approximately 40 minutes/sample in comparison to ~20 seconds/sample in all other conditions).

[11]Prusa MK3S+: https://www.prusa3d.com/product/original-prusa-i3-mk3s-3d-printer-mmu3-kit-bundle/

[12]MTS Exceed E43.504 Universal Testing Machine: https://www.mts.com/en/products/materials/static-materials-test-systems/exceed-electromechanical

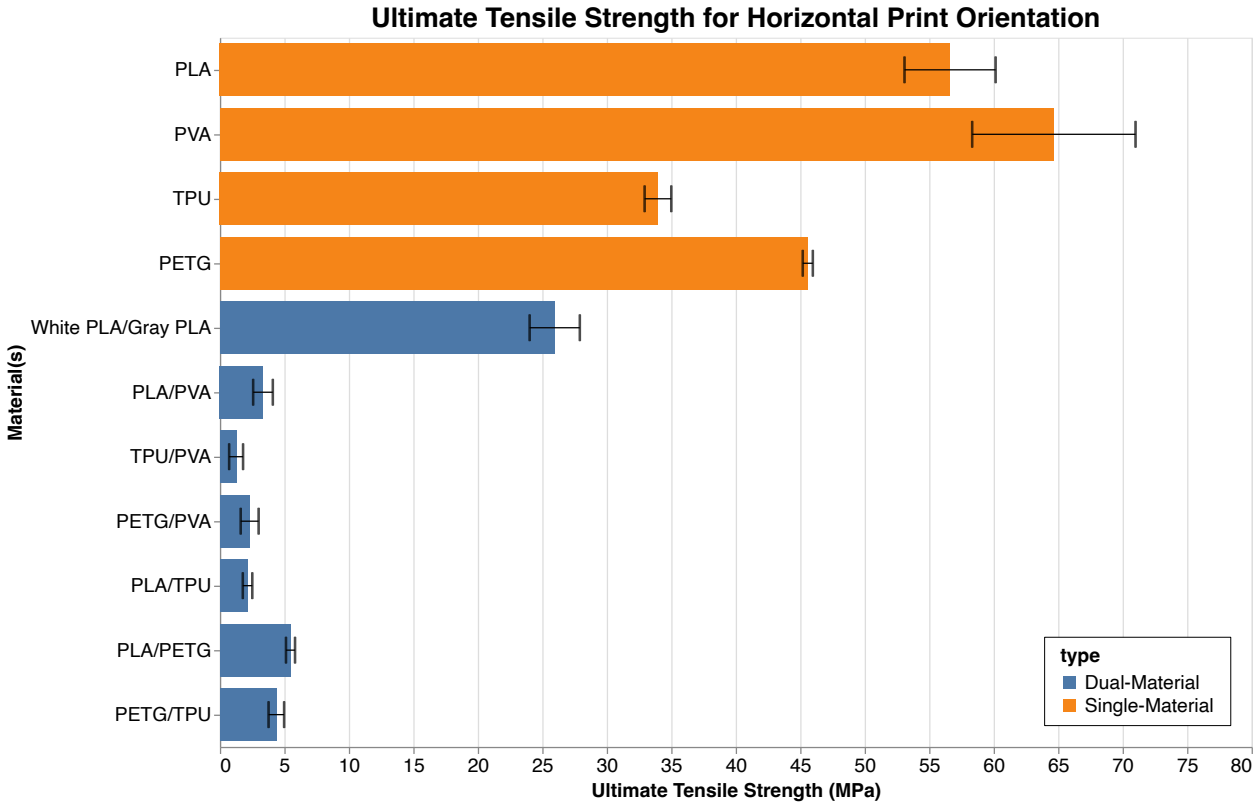

Figure 5: Ultimate tensile strength (UTS) test results for single-material and dual-material with a plain interface with a horizontal print orientation showing the mean of five samples per condition. Error bars indicate the standard deviation. UTS of dual-material with a plain interface drops significantly compared to UTS of each of the materials by themselves.

4.1.4 Results - Horizontal Print Orientation. The results of the ultimate tensile strength (UTS) tests for different material combinations with a horizontal print orientation are shown in Figure 5. The strengths of the single-material conditions are comparable to generally accepted values [79]. Their strengths are also significantly higher than any dual-material conditions (both plain and slot joint interfaces). Even the same material printed side-by-side in two parts—the *white PLA/gray PLA* condition (μ: 25.96 MPa, SD: 1.95)—has a much lower UTS compared to that of itself printed as single material (*PLA* – μ: 56.62 MPa, SD: 3.53). The strengths drop even further for other dual-material conditions with a plain interface (no slot joint interfaces) between two different materials; the results are all below 6 MPa.

The results for different interface geometries are shown in Figure 6. All PLA/PVA dual-material conditions with slot joint interfaces had strength higher than their plain interface counterparts (PLA/PVA *Plain* – μ: 1.71 MPa, SD: 1.21), and in some cases more than twice the strength, for example, *M2r* (μ: 10.31 MPa, SD: 2.30) and *M2rh* (μ: 11.80 MPa, SD: 1.47). All of these samples broke at the interface of the two materials. We speculate that the strength increased because more force is needed to overcome adhesion at the middle of the interface and between the slots joints and their surrounding material as is suggested by broken slots joints at the rupture sites shown in Figure 4d.

For the different slot joint types, increasing the number of slots also increased the strength. For example, the condition with 6 cylindrical slots extended from both materials, 12 slots in total (*C6b* – μ: 6.50 MPa, SD: 0.27), has almost twice the strength of the condition with 6 cylindrical slots from only one material (*C6* – μ: 3.95 MPa, SD: 0.15). This is likely due to the additional slot joints increasing the contact area between the two materials. For the mushroom-shaped slot joints, similar cross-section area of the slot joints achieves similar strength as demonstrated by the two mushroom (*M2* – μ: 6.88 MPa, SD: 1.08) and three mushroom (*M3* – μ: 5.78 MPa, SD: 0.79) slots conditions.

Other parameters that increase either contact surface area or cross-sectional area of the slots also increase strength. For example, a slot radius of 2.0 mm (*M2r* – μ: 10.31 MPa, SD: 2.30) results in higher strength than a slot radius of 1.5 mm (*M2* – μ: 6.88 MPa, SD: 1.08). Similarly, increasing the stem length from 2.5 mm (*M2r* – μ: 10.31 MPa, SD: 2.30) to 7.5 mm (*M2rh* – μ: 11.80 MPa, SD: 1.47) also slightly increased the strength, with all other parameters remaining the same.

We also tested one of the strongest interface geometries from the PLA/PVA tests—the two mushroom-shaped slot joints with a

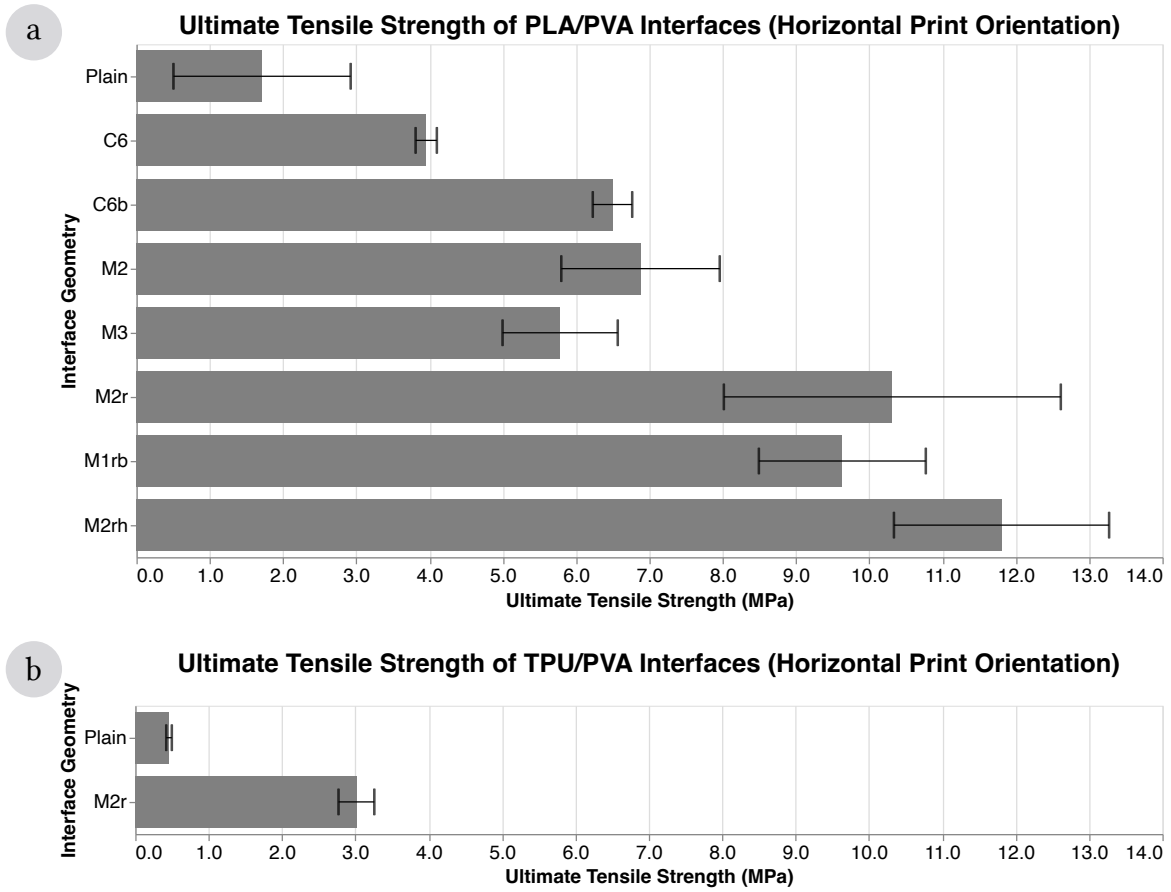

Figure 6: Ultimate tensile strength (UTS) test results for different interface geometries with a horizontal print orientation showing the mean for five samples per condition. Error bars indicate the standard deviation. (a) UTS of PLA/PVA samples with eight different interface geometries. (b) UTS of TPU/PVA samples with a plain interface and an interface with two mushroom-shaped slots.

stem radius of 2 mm (*M2r* – μ: 3.01 MPa, SD: 0.24) on the TPU/PVA combination. This result is much higher than that of TPU/PVA with a plain interface (μ: 0.46 MPa, SD: 0.04).

4.1.5 Results - Vertical Print Orientation. The UTS results for the vertical print orientation conditions and their horizontal counterparts are shown in Figure 7. All three single-material conditions have much lower UTS when printed vertically than horizontally. For example, the PLA vertical UTS (μ: 40.59 MPa, SD: 2.16) is lower than its horizontal UTS (μ: 56.62 MPa, SD: 3.53). Likewise, the PVA vertical UTS (μ: 6.92 MPa, SD: 0.72) is significantly lower than its horizontal UTS (μ: 64.67 MPa, SD: 6.33). This is in alignment with prior work [22, 43]. Notably, when TPU and another material have a plain interface, the vertical conditions have a comparable or even higher UTS than that of horizontal conditions. For example, the TPU/PVA vertical UTS (μ: 1.37 MPa, SD: 0.61) is higher than its horizontal UTS (μ: 0.46 MPa, SD: 0.04). In these tests, TPU was printed on top of another material to minimize any potential print instabilities from the object flexing during printing. We hypothesize that this may have enabled better bonding between the interface layers of the samples. Finally, the vertical slot interfaces have comparable or higher strength to their vertical plain interface counterparts. For example, the vertical *M2r* slot interface with PLA/PVA (μ: 1.04 MPa, SD: 0.39) has higher UTS than the plain PLA/PVA interface (μ: 0.86 MPa, SD: 0.50). The vertical TPU/PVA *M2r* slot interface (μ: 1.14 MPa, SD: 0.23) is marginally weaker than the vertical plain TPU/PVA (μ: 1.37 MPa, SD: 0.61). Across these results, the vertical slot interfaces when compared to the vertical plain interfaces did not significantly increase the attachment strength as much as the horizontal slot interfaces did relative to the horizontal plain interfaces.

4.1.6 Summary. The results of these tests offer several important findings. First, the strength between PVA and different materials is slightly lower than the materials when bonded to each other. Second, slot joints can generally increase the strength of adhesion between PVA and other materials to be much higher than the adhesion of the materials bonded to each other using a plain interface (which is common in multi-material 3D printing) when the slots are printed in a horizontal orientation. When printed vertically,

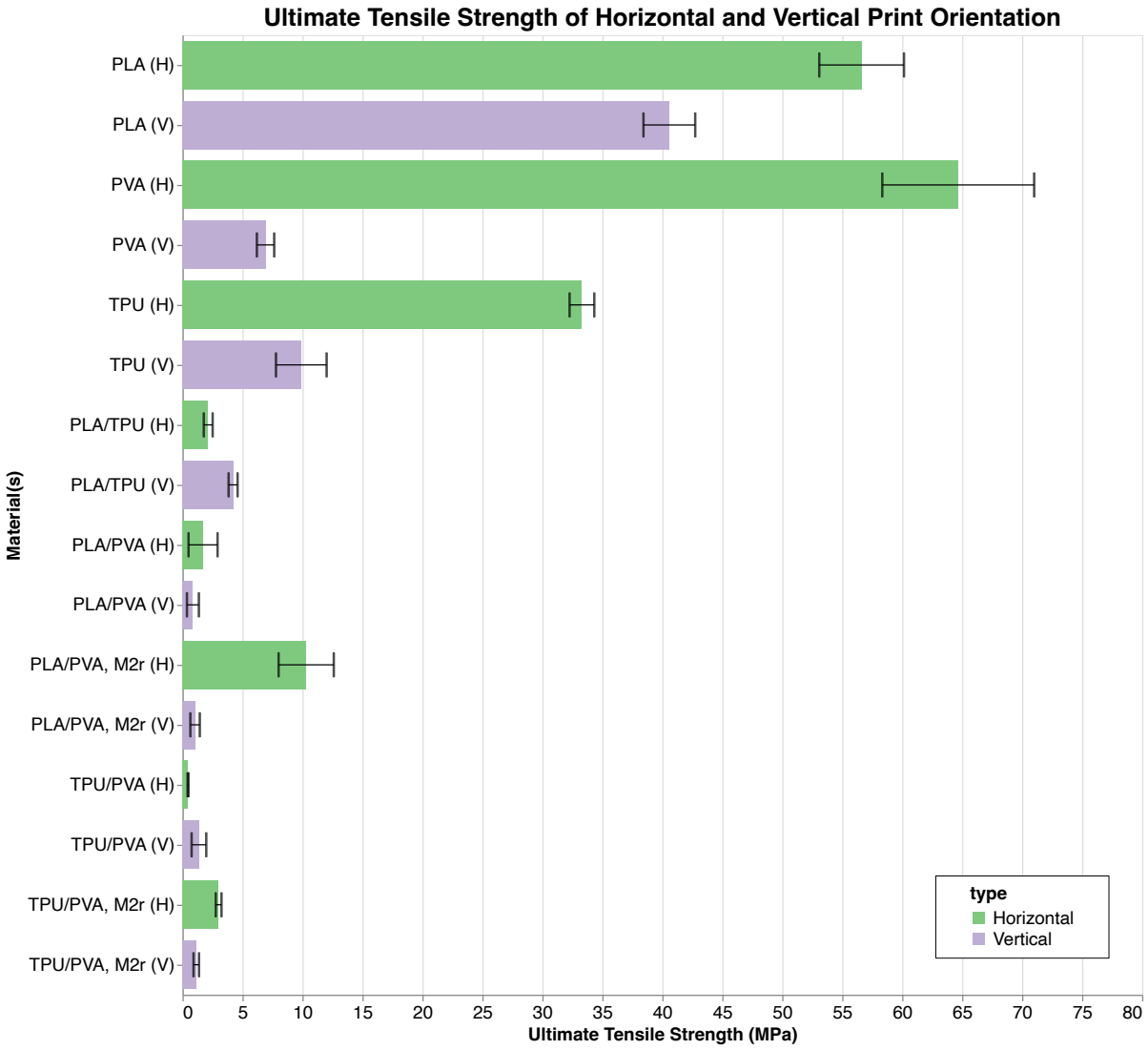

Figure 7: Ultimate tensile strength (UTS) test results for horizontal and vertical print orientation showing the mean for five samples per condition. Error bars indicate the standard deviation. UTS of vertically printed samples are in general lower than that of their horizontally printed counterparts except for PLA/TPU and TPU/PVA with a plain interface.

the effect of slots is reduced. With this in mind, our computational approach offers the flexibility to choose whether the generated dissolvable interfaces should be plain to minimize the use of interface material, or have slot joints to maximize strength between different materials, subject to the print orientation as is typical in 3D printing.

4.2 Shear Strength

To further evaluate whether adding PVA interfaces impacts the strength between different materials in other loading conditions, we conducted shear strength tests according to ASTM standard D3164-03 [5]. An overview of the tests is shown in Figure 8.

4.2.1 Test Conditions. We tested three conditions: PLA/TPU directly bonded to each other; PLA/TPU bonded by a PVA plain interface; and PLA/TPU bonded by a PVA slots interface. The PLA/TPU bonded to each other condition provides a baseline for the shear strength between the two materials. The other two conditions evaluate the impact of PVA interfaces on shear strength. For all three conditions (Figure 8a), the cross-section of the bond area is 25.4 mm by 12.7 mm, and the PLA and TPU portions of the specimen are each 101.6 mm by 25.4 mm by 3 mm with an additional spacer region (25.4 mm by 25.4 mm by 4 mm) to support the specimen in the test machine's grippers. The PVA plain interface has a thickness of 1 mm. The PVA slot interfaces have a base with a thickness of 1 mm and 7 mushroom slots on each side protruding into the PLA

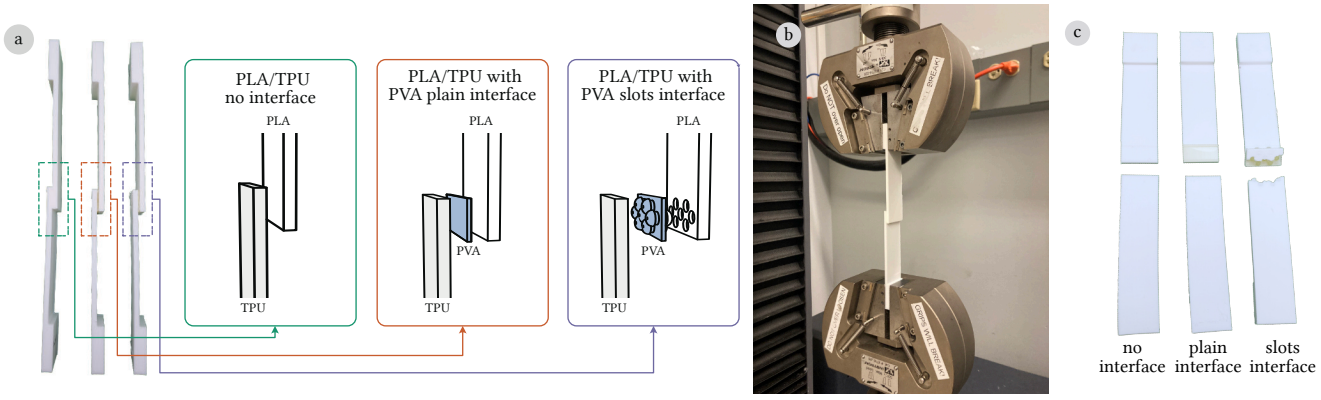

Figure 8: Overview of the shear strength tests. (a) Test specimens for the three testing conditions: PLA/TPU with no interface (left), PLA/TPU with plain PVA interface (middle), PLA/TPU with a mushroom slot PVA interface (right); (b) Experimental apparatus for the ASTM standard D3164-03 shear strength test; (c) Example rupture sites for the three test conditions.

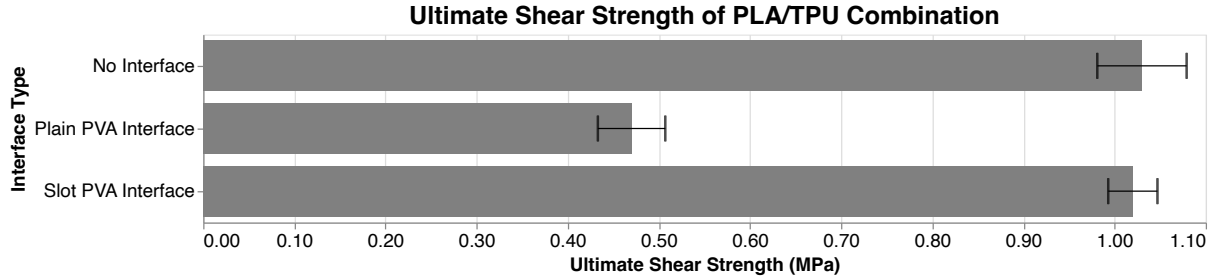

Figure 9: Ultimate shear strength (USS) test results for PLA/TPU bounded by different interfaces showing the mean for five samples per condition. Error bars indicate the standard deviation. USS of PLA/TPU bounded by PVA slot interface is nearly identical to that of PLA/TPU bounded to each other.

and TPU material. The mushroom slots have the same slot radius and cap radius as the the tensile strength test's *M2r* interface condition, which yielded high strength tensile strength. However, the slot height is reduced to 1 mm and cap height to 1.25 mm so the mushroom slots are contained within the PLA and TPU regions. We increased the number of mushroom slots to 7 to maintain the same ratio of slot cross-sectional area to overall bond area (0.27) as the ratio used in the *M2r* condition of the tensile strength test.

4.2.2 Sample Preparation. For each condition, we tested five samples (N=5). All samples were sliced in PrusaSlicer with a horizontal print orientation, 100% rectilinear infill at 45° angle, and a layer height of 0.2 mm. The samples were printed on a Prusa XL with Overture PLA (white), Overture TPU (white), and Fused Materials PVA.

4.2.3 Test Apparatus and Procedure. Tests were performed using an MTS Exceed E43.504 Universal Testing Machine with a 50 kN load cell (Figure 8b). All tests were conducted with a 0.022 mm/s crosshead speed.

4.2.4 Results. The ultimate shear strength (USS) results for the three conditions are shown in Figure 9. The USS for the PLA/TPU condition is 1.03 MPA (SD: 0.05). The bond failed between the two materials such that the PLA and TPU peeled off one another. The USS for the PLA/TPU with a PVA plain interface is 0.47 MPA (SD: 0.04) and the bond failed at the interface between PLA and PVA. Lastly, the USS for the PLA/TPU with PVA slot interface is 1.03 MPA (SD: 0.03) and the failure occurred within the PLA material itself as shown in Figure 8c.

4.2.5 Summary. Overall, the shear strength of the plain PVA interface between PLA and TPU is weaker than when the materials are bonded with no interface. However, the addition of slot joints in the PVA interface makes its shear strength just as strong.

4.3 Water Dissolution

We performed a water dissolution test (Figure 10) to better understand how quickly PVA dissolves in different conditions.

4.3.1 Test Conditions. Our test consisted of two conditions PVA-only and PVA partially enclosed by PLA. The PVA-only condition is used to establish a baseline for PVA dissolution. The enclosed condition demonstrates dissolution when the PVA is partially enclosed by another material as is the case when using a dissolvable interface between other materials.

For each condition, the amount of PVA used was held constant (Figure 10a). The PVA portion in both conditions was tube-shaped,

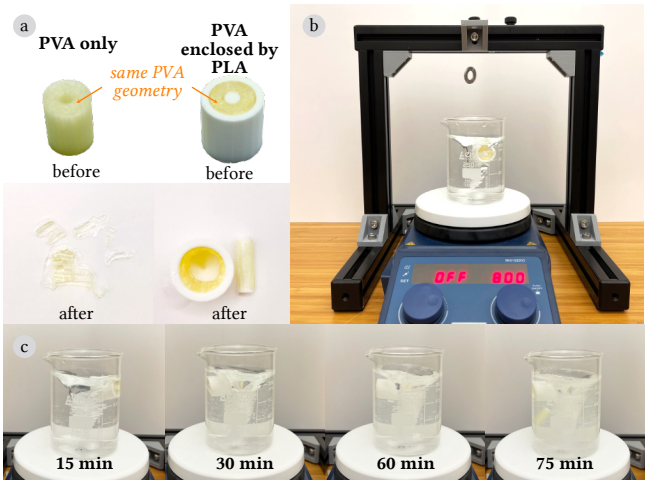

Figure 10: Water dissolution test set-up and results for PVA. (a) Samples for the two dissolution testing conditions: PVA only and PVA partially enclosed by PLA; PVA only sample before (top left) and after (bottom left) the test, and PVA partially enclosed by PLA sample before (top right) and after (bottom right) the test are shown. (b) A sample is suspended with a monofilament fishing line inside a beaker containing 200 mL of room temperature water. (c) The water is agitated at 800 RPM using a magnetic stirrer plate for up to 75 minutes to progressively dissolve the sample.

consisting of a cylinder (20 mm height, 7.5 mm radius) with a cylindrical hole cut (2.5 mm radius) from its center. This shape was chosen to ensure printabilty and that water could uniformly dissolve the PVA around the tube's radius. For the enclosed PVA condition, the cylindrical hole was filled by a PLA cylinder (2.5 mm radius) and the outer PVA cylinder was surrounded by PLA (2.5 mm thick).

4.3.2 Sample Preparation. For each condition, we printed five (N=5) samples. Samples were sliced in PrusaSlicer using a 20% rectilinear infill at a 45° angle with 0.2 mm layer height. All samples were printed using a Prusa XL with white Overture PLA and Fused Materials PVA.

4.3.3 Test Apparatus and Procedure. Figure 10b shows our experimental setup. For each sample, we recorded its initial mass in grams (g). We filled a 250 mL beaker with 200 mL of room-temperature tap water and placed a magnetic stirrer (40 mm in length) at the bottom. The beaker was placed on top of a stirrer plate, which is directly below a metal fixture. Using a monofilament fishing line, each sample was then suspended from the fixture such that it was fully submerged in the water (approximately 40 mm from the bottom of the beaker). We tied a M10 washer approximately 80 mm above the sample and outside the beaker to add tension on the line.

We set the stirrer rate to 800 RPM and ran the test until the sample separated from the fishing line or 75 minutes had elapsed (Figure 10c). In either case, we recorded the dissolution time. The sample was then removed from the beaker and left to fully dry. We then recorded the undissolved mass of the sample in grams.

4.3.4 Results. For PVA-only condition, the average initial mass was 2.03 g (SD: 0.011). In all five tests, the PVA-only sample separated from the fishing line before 75 minutes elapsed. The average dissolution time is 48.3 min (SD: 1.41). The average loss in mass is 1.67 g (SD: 0.066), or 82.3% of the initial mass. The average rate of dissolution is 0.035 g/min (SD: 0.0023).

For the enclosed PVA condition, the average starting mass was 5.08 g (SD: 0.011). All five tests ran for the full 75 minutes. The average loss in mass is 0.822 g (SD: 0.134), or 16.2% of the initial mass. The average rate of dissolution is 0.011 g/min (SD: 0.0018). As expected, the rate of dissolution for enclosed PVA is lower, approximately one-third that of PVA-only. This is because the PVA surface area that is initially exposed to water is also much lower, with the enclosed PVA surface area (314.16 mm^2) being approximately five times lower than PVA-only (1570.80 mm^2).

4.3.5 Summary. Increasing the surface area of the PVA exposed to water will generally increase the rate of dissolution. However, this relationship is not linear because the exposed surface area changes as more PVA is dissolved over time. As long as the PVA is not fully encased in another material, it will dissolve over time.

5 Example Demonstrations

To demonstrate our computational technique, we processed and fabricated nine objects that have different structural, functional and aesthetic qualities. Several of these examples were existing multi-material 3D models sourced from online repositories such as Thingiverse[13] and Printables[14]. All of the objects were printed on a 5-tool Prusa XL using various combinations of PLA, conductive PLA, PETG, TPU, and PVA. Only the dissolvable interfaces were printed in PVA. After fabrication the objects were submerged in water for at least 16 hours to demonstrate the disassembly process that enables recycling at their end of life. We summarize object information in Table 4 and the results of disassembly by dissolution in Table 5. Full interface generation parameters for each object can be found in Table A, Table 6. We also provide print time information in Appendix A, Table 7.

5.1 Striped Lizard

The striped lizard [18] is a tri-color 3D model available on Thingiverse. It has several interesting geometric features including non-planar surfaces where different colors of the lizard's body meet; partially nested structures (e.g., the eyes); and small parts such as its toes. We produced and fabricated two versions of the lizard using blue, green and yellow PLA. We first generated a plain interface version, which took 188.9 seconds, however, some of the smaller parts (e.g., end of the tail and some toes) broke off at their interfaces while removing the fabricated object from the printer. This suggested that the plain interfaces did not provide enough strength in areas where small parts meet. We generated the second version with cylindrical slots (Figure 1), which took 229.4 seconds. This version of the object stayed intact while being removed from the printer. After dissolution, all of this object's non-dissolved materials were fully separated. This represents 81.58% of the object's original mass, where the remaining 18.42% was dissolved PVA.

[13]Thingiverse: https://thingiverse.com
[14]Printables: https://printables.com

Object Information					Interface Parameters		Processing Time (s)		
Name	*Input STLs*	*Mesh Vertices*	*Mesh Faces*	*Mesh Volume (mm^3)*	$t_{interface}$ *(mm)*	*Interface Type*	*Interface Generation*	*Interface Cutting*	*Total*
striped lizard	3	222,487	369,252	35,583	1.0	cylindrical	48.6	180.8	229.4
plant cell	4	100,758	157,918	75,685	1.0	plain	568.7	1353.4	1922.1
tongs	2	1,644	1,360	30,357	1.0	cylindrical	11.5	37.5	49.0
candy cane	2	20,340	23,576	1,723	0.6	plain	14.6	87.1	101.7
hair brush	2	20,206	36,512	70,500	1.0	cylindrical	19.4	167.7	187.1
bag holder	2	17,295	28,964	153,944	1.0	mushroom	28.5	45.5	74.0
sheep	3	86,930	163,788	163,788	0.8	plain	40.5	31.7	72.2
fidget toy	2	5,507	7,960	102,058	1.0	plain	29.2	36.0	65.2
game controller	4	17,446	26,556	122,003	1.0	plain	68.9	1365.7	1434.6

Table 4: An overview of the example objects and their generated interfaces used to demonstrate our disassembly by dissolution approach. Detailed interface parameters for each object can be found in Appendix A, Table 6.

5.2 Plant Cell

The plant cell [57] is a model for science education available on Thingiverse that uses different colors to illustrate a plant cell's various components. In terms of geometry, the model has several small thin-walled parts and nested components. We generated plain interfaces for the object (Figure 11), which took 1922.1 seconds. The object's components were then fabricated using green, yellow, red, and blue PLA. After dissolution, all of the object's components were fully separated, accounting for 87% of the object's original mass. The remaining 13% of the mass was dissolved PVA.

5.3 Tongs

We created a two-material 3D model of a pair of tongs that is intended to have flexible teeth for gripping and a rigid handle. Because the teeth rest on the object's surface and need to withstand forces from gripping objects, we generated cylindrical slot interfaces to increase attachment strength (Figure 12), which took 49.0 seconds.

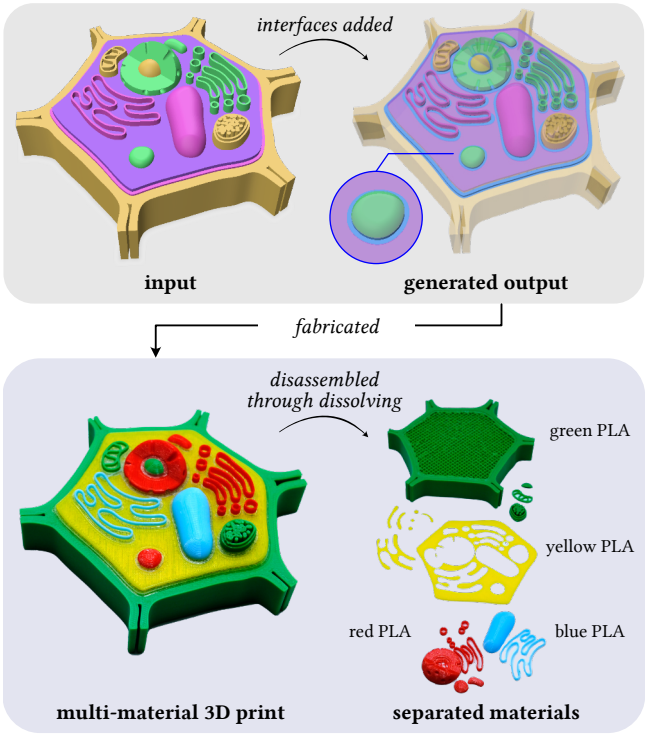

Figure 11: The plant cell model when processed, fabricated, and fully disassembled.

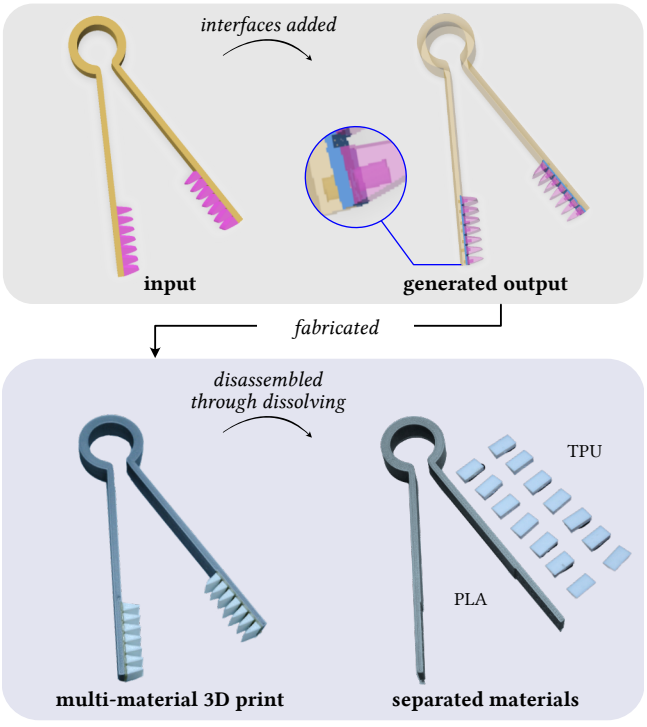

Figure 12: The pair of tongs when processed, fabricated, and fully disassembled.

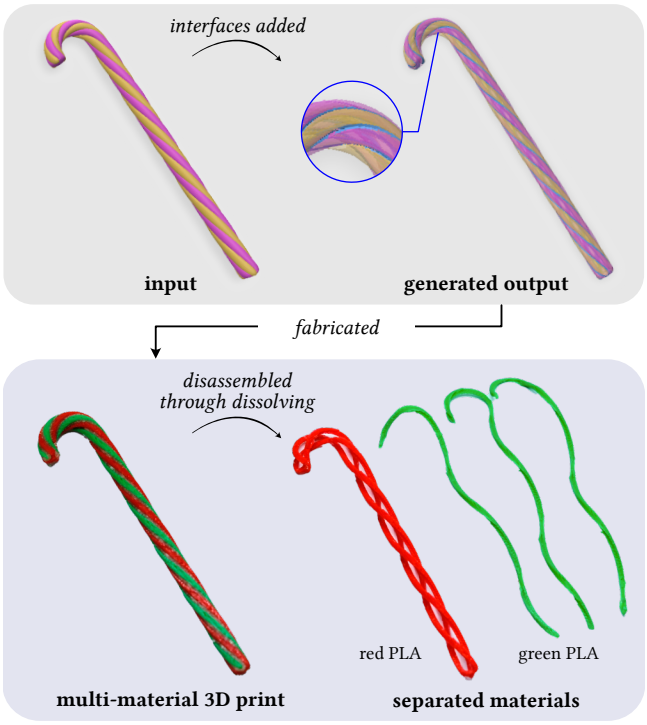

Figure 13: The candy cane model when processed, fabricated, and fully disassembled.

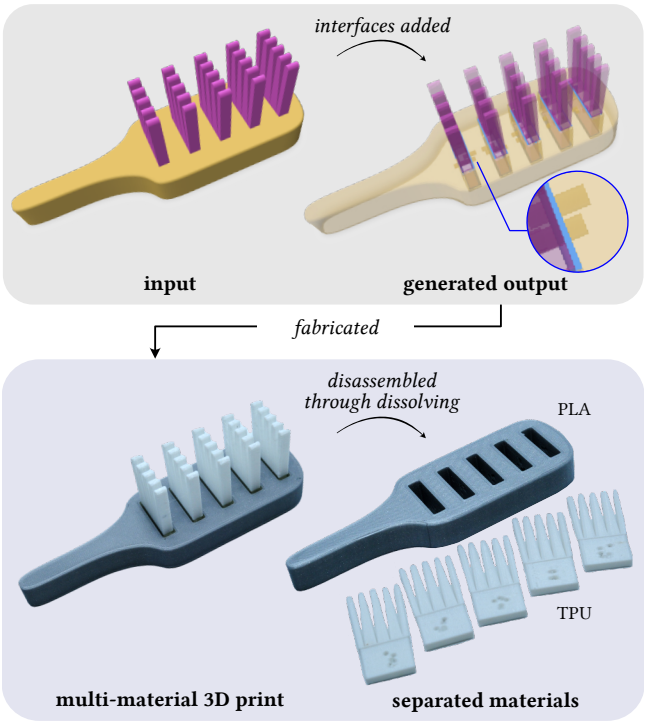

Figure 14: The hair brush when processed, fabricated, and fully disassembled.

The object's components were then fabricated using white TPU for the teeth and gray PLA for the handle. After dissolution, all of the object's components were fully separated, accounting for 92.66% of the object's original mass. The remaining 7.34% of the mass was dissolved PVA.

5.4 Candy Cane

The candy cane [26] is a holiday ornament available on Printables. Its geometry consists of three spiral strands interwoven around a twisted core. We generated plain interfaces for the object (Figure 13), which took 101.7 seconds. Because of the candy cane's intertwined components and small diameter (~4.7 mm), we used a small interface thickness of 0.6 mm to preserve the original object's aesthetics. The object was fabricated using red and green PLA. After dissolution, all of the object's components were separated. However, some agitation was needed to dislodge the individual green strands as they were still held by friction within the twisted core. Of the object's original mass, 60.87% was accounted for in the separated materials with the remaining 39.13% being dissolved PVA.

5.5 Hair Brush

We created a hair brush that has a rigid handle and flexible bristles. In contrast to the tong's teeth, the bristles are partially nested within the handle to provide additional support during use. We generated cylindrical slot interfaces to increase attachment strength (Figure 14), which took 187.1 seconds. The object was then fabricated using white TPU for the bristles and gray PLA for the handle. After dissolution, all of the object's components were fully separated, accounting for 85.45% of the object's original mass. The remaining 14.55% of the mass was dissolved PVA.

5.6 Bag Holder

We designed a bag holder that has flexible grips for comfort, and a durable body for holding heavy bags. To provide additional attachment strength during use, we generated mushroom slot interfaces (Figure 15), which took 74.0 seconds. The object was then fabricated using white TPU for the grips and orange PETG for the handle. After dissolution, all of the object's components were fully separated, accounting for 95.39% of the object's original mass. The remaining 4.61% of the mass was dissolved PVA.

5.7 Interactive Sheep

We created a multi-part sheep model that has a conductive trace internally routed through its body to its face (Figure 16). This trace acts as a capacitive touch sensor to support interactivity. In terms of geometry, the sheep has several structures that are nested within one another such as its pupils nested within its eyes, which are then nested within its head. In addition, the conductive trace is routed through different structures (head, body) that also represent different materials (conductive and non-conductive). We generated plain interfaces for the sheep, which took 72.2 seconds. After dissolution, all of the object's non-dissolved materials were fully separated. This

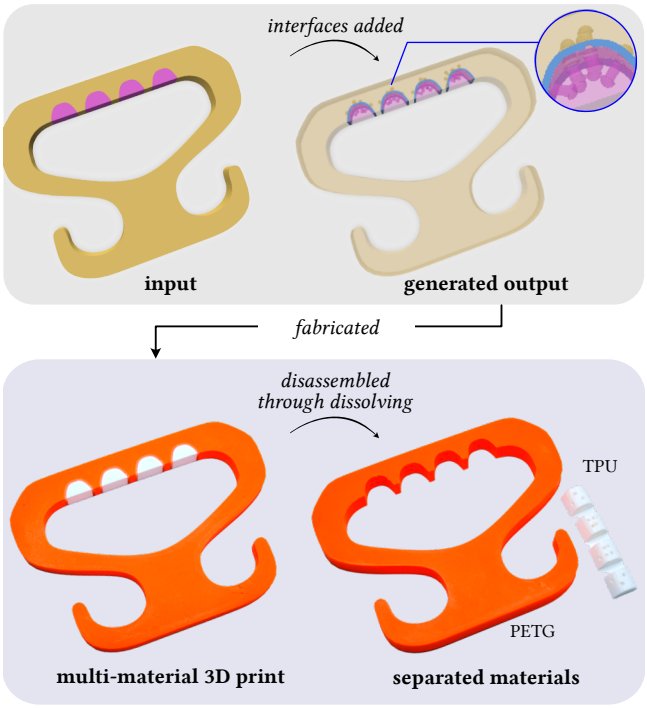

Figure 15: The bag holder when processed, fabricated, and fully disassembled.

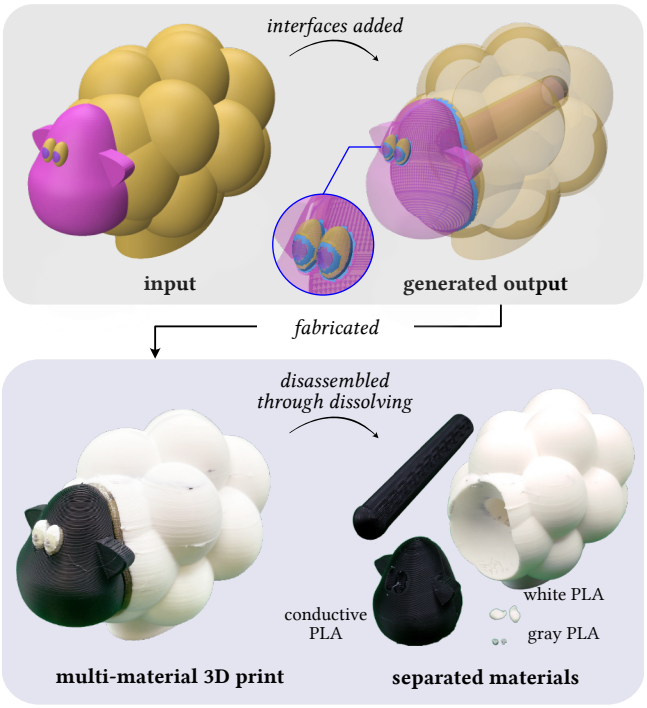

Figure 16: The interactive sheep when processed, fabricated, and fully disassembled.

represents 93.01% of the object's original mass, where the remaining 6.99% was dissolved PVA.

5.8 Fidget Toy

We designed a fidget toy featuring a rigid enclosure and soft custom-shaped buttons that protrude above the enclosure's surface. During use, the buttons will experience downward force when pressed (as opposed to laterally as with the hair brush's bristles). Thus, the object does not need slots for additional attachment strength. We generated plain interfaces (Figure 17), which took 65.2 seconds. The object was then fabricated using gray PLA for the enclosure and white TPU for the buttons. After dissolution, all of the object's components were fully separated, accounting for 90.2% of the object's original mass. The remaining 9.8% of the mass was dissolved PVA.

5.9 Interactive Game Controller

We designed a game controller with flexible interactive buttons and a directional-pad embedded into a two-color rigid enclosure. Similar to the interactive sheep, each button has an internally-routed conductive trace. We generated plain interfaces for the controller, which took 1434.6 seconds. The object was then fabricated using gray and blue PLA for the case, white TPU for the buttons, black conductive PLA for the internal traces. After dissolution, all of the object's components were fully separated, accounting for 87.53% of the object's original mass. The remaining 12.47% of the mass was dissolved PVA.

6 Discussion and Limitations

6.1 Interface Generation Considerations and Constraints

Choosing an appropriate dissolvable interface is crucial to preserving the functionality and visual appearance of a multi-material 3D printed object. All of our example demonstrations have interface thicknesses of 1 mm except the candy cane which has an interface thickness of 0.60 mm. When too large of a thickness is chosen, more material in the original object is converted into a dissolvable interface. For small objects (such as the candy candy) or objects with very small features (<1 mm^2) located where two materials meet, too large of an interface thickness can cause a drastic change in appearance. At the same time, if too small of an interface thickness is chosen, the interface may not be printable. We recommend the interface thickness be at least the extrusion width of the 3D printer used for fabricating an object (typically between 0.4 to 0.5 mm). However, choosing a value that is approximately twice this number ensures printability and is more robust to any potential printing artifacts.

Relatedly, the type of interface—plain, with cylindrical slots, or with mushroom-shaped slots—should be selected based on the intended use of an object. Our tensile strength and shear test results indicate that the plain interface (no slot joints) has the lowest overall strength, but is of similar magnitude to the bond strength between different materials without any interface added. In addition, the plain interface utilizes the least amount of dissolvable material

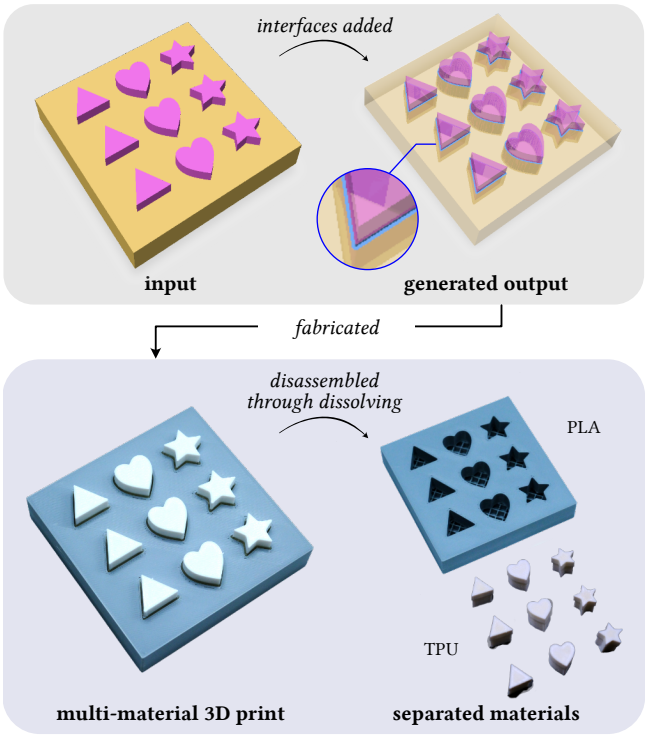

Figure 17: The fidget toy when processed, fabricated, and fully disassembled.

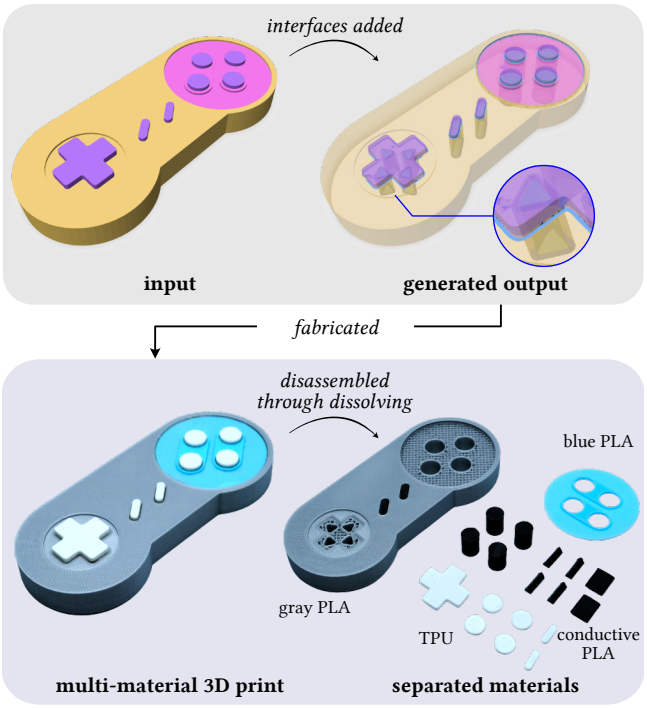

Figure 18: The game controller when processed, fabricated, and fully disassembled.

compared with the other two interface types and therefore takes less time to dissolve for disassembly.

The plain interface is most useful in applications that are for aesthetic purposes and do not require strong connections between different materials (e.g., when one structure is nested within another). Both the game controller and the interactive sheep have conductive traces that are enclosed within an outer structure. In these examples, the outer structure already provides significant support for the inner material so plain interfaces are sufficient.

In most cases, adding slot joints can significantly increase the strength of the bonds between interfaces and their adjacent materials. Though, this effect is mediated by print orientation. Adjusting the generation parameters of an interface can further impact the strength. A larger size and/or an increased number of slot joints are both associated with higher strength. However, slot joints also come with trade-offs. Slot joints replace more material in the original model with a dissolvable interface, potentially changing the object's aesthetics. This is more apparent with mushroom-shaped slot joints as they can potentially appear on an object's surface (e.g., on the feet of the lizard example). Likewise, more interface material can increase the dissolution time for disassembly.

Both the flexible grips of the bag holder and the bristles of the brush are intended to experience strong forces during use. Thus, we chose to maximize strength by using interfaces with mushroom-shaped slots and cylindrical slots, respectively. Across all of our examples, we considered strength, aesthetics, and speed of dissolution when choosing an interface type. We recommend balancing these factors when choosing a dissolvable interface for any application. Currently, these considerations must be manually weighed by a user. However, we believe there is an opportunity to leverage physically-based simulation and optimization in this process. Our tensile and shear tests provide a baseline strength characterization for different materials, interface conditions, and print orientations. When combined with user input regarding an object's intended use (e.g., loading conditions), such a tool could determine the optimal interface geometry for a given application. Likewise, it could be used to examine the anticipated dissolution and disassembly of the object prior to its end-of-life.

6.2 Recycling 3D Printed Materials

Across all 9 multi-material objects, our approach enables 89.97% (339.66 g) of the total mass of their materials to be recycled. These materials can be easily separated and sorted by type and color. Likewise, dissolved interfaces made from PVA could also be recycled using existing techniques [25, 30]. If the PVA is recycled, our approach supports recycling of *all* the materials in these multi-material 3D printed objects. However, we note that PVA recycling is not widely available [30, 72].

It would be ideal if all thermoplastic materials used in 3D printing could be recycled through a typical municipal recycling program, but the reality is that the infrastructure to identify, separate and sort these materials does not currently exist [55, 97]. As of now, recyclers of 3D printed plastics such as TerraCycle [84] and Printerior [66] require individuals to separate, label and ship materials to their

	Disassembly by Dissolution Results						
Name	*Dissolution Time (hours)*	*Original Mass (g)*	*Dissolved Interfaces Mass (g)*	*Unseparated, Non-Soluble Mass (g)*	*Separated, Non-Soluble Mass (g)*	*Dissolved PVA Mass %*	*Recylable, Non-Soluble Mass %*
striped lizard	40	23.40	4.31	0	19.09	18.42	81.58
plant cell	15	32.69	4.25	0	28.44	13.00	87.00
tongs	16	23.15	1.70	0	21.45	7.34	92.66
candy cane	16	1.61	0.63	0	0.98	39.13	60.87
hair brush	24	44.54	6.48	0	38.06	14.55	85.45
bag holder	40	71.29	3.29	0	68.00	4.61	95.39
sheep	43	73.51	5.14	0	68.37	6.99	93.01
fidget toy	39	49.89	4.89	0	45.00	9.80	90.20
game controller	44	57.43	7.16	0	50.27	12.47	87.53

Table 5: Results of dissolving the example objects. All objects were fully disassembled and their non-soluble materials can be recycled. The combined recyclable non-soluble material amounts to 89.97% (339.66 g) of the combined mass of all the objects.

facilities. Our approach unlocks these recycling processes for multi-material 3D printed objects.

In addition, our approach supports growing efforts in do-it-yourself filament recycling with machines such as the Recreator3D [41] and the ARTME 3D Desktop Filament Extruder [3]. Recycling multi-material 3D printed objects with these machines can empower individuals and community makerspaces to create sustainable digital fabrication practices that encourage the use of locally recycled materials.

6.3 Interface Dissolvability and Its Impact on Functionality

Our computational approach makes no assumptions about the particular materials used in a 3D printing process. As a result, the generated output should work with any materials as long as the interface material is dissolvable, and its dissolution process does not impact the quality of other materials for recycling. Crucially, a dissolvable interface material should be selected based on an object's intended use. In this work, we demonstrated using PVA as an interface material. In terms of longevity, our example objects have been handled by dozens of individuals over several months with no apparent change in their functionality. Likewise, the adhesion between materials does not appear to have affected by a low-moisture environment. However, this may not the case in high humidity environments. Because PVA is water-soluble, it is not suitable to be used in applications that require high moisture or contact with water (e.g., a boat). Other dissolvable 3D printing materials such as HIPS (soluble in d-limonene [36]) and polyvinyl butyral[15] (soluble in isopropyl alcohol), would likely be a better choice for objects with water-based applications.

6.4 Challenges with Disassembly by Dissolution

A key goal in this work is to support disassembly by dissolution, however, some objects may still require additional geometry modifications to enable disassembly, or need some mechanical effort to separate different materials. Consider a small sphere inside of a larger sphere (e.g., a model of the earth with its core within) as in Figure 19. In this case, our algorithm would produce an interface around the inner sphere (the core). However, during the dissolution process even if water made its way through the outer sphere's layer lines to dissolve the interface, there would be no way for the inner sphere to separate as it is trapped inside. Thus, it would be necessary to segment, or add a "split" through the outer sphere's geometry to integrate another interface that could effectively split open the outer sphere during dissolution. Once this interface is dissolved, the outer sphere would then separate, providing a way for the inner sphere to exit. These splits could be computationally-generated using a part segmentation approach (e.g., [48, 59]). However, some 3D models may necessitate a user suggesting a splittable region as input to the system to avoid the possibility of potential splits and interface generation compromising an object's functionality (e.g., print-in-place movable joints).

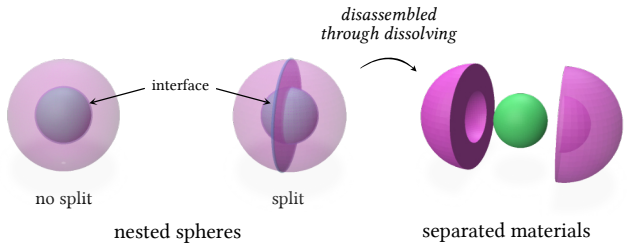

Figure 19: Rendered example showing that components which are completely encapsulated inside of an object such as nested spheres will not separate without a split being added to the outer geometry.

Similarly, an object may also have different colors or materials that are heavily woven together such as the candy cane in Figure 13. After its interfaces are dissolved, the object's pieces may still be somewhat interlocked. In such cases, the disassembly process may require mechanical intervention (e.g., agitation using a water circulation pump) to unweave the parts from one another.

[15] Polyvinyl butyral (PVB): https://all3dp.com/2/pvb-filament-simply-explained/

Industrial-scale plastic recycling processes already use techniques such as air-blown pressure to forcefully separate different plastic materials [77]. Similar approaches could be used to disassemble and sort multi-material 3D printed plastics once the interfaces are dissolved.

7 Future Work

7.1 Sustainable Alternative Interface Materials

Prior work emphasizes the largest environmental impact benefits resulting from using materials that are bio-based, renewable, recyclable and low-/no-temperature materials for 3D printing [23, 24, 69]. PVA is recyclable [25, 30] and technically biodegradable [31, 32]. However, its recycling processes are not widely used [30, 72], and its biodegradation is slow and depends on specific microorganisms that are not common in the U.S. Wastewater Treatment Plants or the environment [72]. Thus, it is important to find more sustainable materials that exhibit similar strength, dissolvability, and adhesion as PVA. Several dissolvable bio-based materials such as agar-agar [7] and gelatin [44, 45] could provide more sustainable alternatives to PVA if they could be adapted into 3D printing materials. Likewise, replacing all thermoplastics used in 3D printing with more sustainable, yet equally functional alternatives is ideal and should be the subject of future work.

7.2 Applying Dissolvable Interfaces to Other Manufacturing Techniques

This work has focused on generating dissolvable interfaces for multi-material objects intended to be fabricated on typical thermoplastic filament-based 3D printers. However, we note that our computational approach is applicable to other multi-material 3D printing processes that support soluble materials such as material jetting (e.g., Stratasys PolyJet[16]). Similarly, dissolvable interfaces could also be used in other multi-material manufacturing processes such as multi-material plastic injection molding, where objects are formed by injecting different molten plastic materials into a single mold [29]. Given that PVA [16] and several other 3D printable thermoplastics (e.g., TPU, ABS) [17] are already injection molded at an industrial-scale, we see an opportunity to leverage dissolvable interfaces as a way to support recycling of objects made through these processes. Future work should evaluate the feasibility of these approaches and their impact on recycling.

8 Conclusion

This work introduces a computational fabrication technique that enables the recycling of multi-material 3D printed objects. This technique generates dissolvable interfaces between different materials in a 3D model without impacting the object's intended functionality. Once the object is fabricated, these interfaces can be dissolved to disassemble the object, and enable various materials to be individually recycled. Our tensile and shear strength evaluation demonstrates that these interfaces are strong—and in some cases, stronger—than the bonds between materials without interfaces. While we illustrate this technique with water-soluble PVA, our computational approach is broadly applicable to any dissolvable 3D-printable material. Through 9 example demonstrations, we show that this approach is highly effective at disassembling objects that are geometrically complex and combine materials that are rigid, flexible, and even conductive. Our technique enables us to recycle 89.97% of the total mass of these objects, leaving only dissolved material behind. As a whole, this work unlocks a new approach that enables recycling in multi-material 3D printing without compromising functionality and has the potential to advance sustainability in other multi-material fabrication techniques.

[16]Stratasys PolyJet Support: https://support.stratasys.com/en/Materials/PolyJet/PolyJet-Support

Acknowledgments

This work is partially supported by the National Science Foundation under Grant #2413631. This work was supported by an agreement with the National Renewable Energy Laboratory (NREL) under Alliance Partner University Program (APUP) No. UGA-0-41026-191. This work was also partially funded by a CU Boulder ATLAS Institute Seed Grant. We would like to thank Sophie Berry for designing the tongs example object. We are also grateful to Rachel Sharpe and the CU Boulder Integrated Teaching and Learning (ITL) Program for their assistance during our tensile and shear tests.

References

[1] Ans Al Rashid and Muammer Koç. 2023. Additive manufacturing for sustainability and circular economy: needs, challenges, and opportunities for 3D printing of recycled polymeric waste. *Materials Today Sustainability* 24 (Dec. 2023), 100529. https://doi.org/10.1016/j.mtsust.2023.100529

[2] Byoungkwon An, Ye Tao, Jianzhe Gu, Tingyu Cheng, Xiang 'Anthony' Chen, Xiaoxiao Zhang, Wei Zhao, Youngwook Do, Shigeo Takahashi, Hsiang-Yun Wu, Teng Zhang, and Lining Yao. 2018. Thermorph: Democratizing 4D Printing of Self-Folding Materials and Interfaces. In *Proceedings of the 2018 CHI Conference on Human Factors in Computing Systems*. ACM, Montreal QC Canada, 1–12. https://doi.org/10.1145/3173574.3173834

[3] ARTME 3D. 2024. Original Desktop Filament Extruder MK2 by ARTME 3D by ARTME 3D | Download free STL model. https://www.printables.com/model/524363-original-desktop-filament-extruder-mk2-by-artme-3d

[4] ASTM International. 2017. ASTM D638-14: Standard Test Method for Tensile Properties of Plastics. https://www.astm.org/d0638-14.html

[5] ASTM International. 2017. Standard Test Method for Strength Properties of Adhesively Bonded Plastic Lap-Shear Sandwich Joints in Shear by Tension Loading. https://www.astm.org/d3164-03.html

[6] S. Sandra Bae, Takanori Fujiwara, Anders Ynnerman, Ellen Yi-Luen Do, Michael L. Rivera, and Danielle Albers Szafir. 2024. A Computational Design Pipeline to Fabricate Sensing Network Physicalizations. *IEEE Transactions on Visualization and Computer Graphics* 30, 1 (Jan. 2024), 913–923. https://doi.org/10.1109/TVCG.2023.3327198

[7] Fiona Bell, Latifa Al Naimi, Ella McQuaid, and Mirela Alistar. 2022. Designing with Alganyl. In *Sixteenth International Conference on Tangible, Embedded, and Embodied Interaction (TEI '22)*. Association for Computing Machinery, New York, NY, USA, 1–14. https://doi.org/10.1145/3490149.3501308

[8] Freddys R. Beltrán, Marina P. Arrieta, Eduardo Moreno, Gerald Gaspar, Luisa M. Muneta, Ruth Carrasco-Gallego, Susana Yáñez, David Hidalgo-Carvajal, María U. de la Orden, and Joaquín Martínez Urreaga. 2021. Evaluation of the Technical Viability of Distributed Mechanical Recycling of PLA 3D Printing Wastes. *Polymers* 13, 8 (Jan. 2021), 1247. https://doi.org/10.3390/polym13081247

[9] Eli Blevis. 2007. Sustainable interaction design: invention & disposal, renewal & reuse. In *Proceedings of the SIGCHI Conference on Human Factors in Computing Systems (CHI '07)*. Association for Computing Machinery, New York, NY, USA, 503–512. https://doi.org/10.1145/1240624.1240705

[10] Robert Bogue. 2007. Design for disassembly: a critical twenty-first century discipline. *Assembly Automation* 27, 4 (Jan. 2007), 285–289. https://doi.org/10.1108/01445150710827069

[11] Alan Brunton, Can Ates Arikan, and Philipp Urban. 2016. Pushing the Limits of 3D Color Printing: Error Diffusion with Translucent Materials. *ACM Trans. Graph.* 35, 1 (Dec. 2016), 4:1–4:13. https://doi.org/10.1145/2832905

[12] Leah Buechley and Ruby Ta. 2023. 3D Printable Play-Dough: New Biodegradable Materials and Creative Possibilities for Digital Fabrication. In *Proceedings of the 2023 CHI Conference on Human Factors in Computing Systems (CHI*

'23). Association for Computing Machinery, New York, NY, USA, 1–15. https://doi.org/10.1145/3544548.3580813

[13] Juris Burlakovs, Mait Kriipsalu, Dmitry Porshnov, Yahya Jani, Viesturs Ozols, Kaur-Mikk Pehme, Vita Rudovica, Inga Grinfelde, Jovita Pilecka, Zane Vincevica-Gaile, Tsitsino Turkadze, William Hogland, and Maris Klavins. 2019. Gateway of Landfilled Plastic Waste Towards Circular Economy in Europe. *Separations* 6, 2 (June 2019), 25. https://doi.org/10.3390/separations6020025

[14] Xuelin Chen, Hao Zhang, Jinjie Lin, Ruizhen Hu, Lin Lu, Qixing Huang, Bedrich Benes, Daniel Cohen-Or, and Baoquan Chen. 2015. Dapper: decompose-and-pack for 3D printing. *ACM Trans. Graph.* 34, 6 (Nov. 2015), 213:1–213:12. https://doi.org/10.1145/2816795.2818087

[15] Tingyu Cheng, Taylor Tabb, Jung Wook Park, Eric M Gallo, Aditi Maheshwari, Gregory D. Abowd, Hyunjoo Oh, and Andreea Danielescu. 2023. Functional Destruction: Utilizing Sustainable Materials' Physical Transiency for Electronics Applications. In *Proceedings of the 2023 CHI Conference on Human Factors in Computing Systems (CHI '23)*. Association for Computing Machinery, New York, NY, USA, 1–16. https://doi.org/10.1145/3544548.3580811

[16] P. Cinelli, E. Chiellini, J. W. Lawton, and S. H. Imam. 2006. Properties of Injection Molded Composites Containing Corn Fiber and Poly(Vinyl Alcohol). *Journal of Polymer Research* 13, 2 (April 2006), 107–113. https://doi.org/10.1007/s10965-005-9012-z

[17] Ciprian Ciofu and Daniel Teodor Mindru. 2013. Injection and micro injection of polymeric plastics materials: a review. *Int. J. Mod. Manufact. Technol* 1 (2013), 49–68. https://ijmmt.ro/vol5no12013/Ciofu_Ciprian_1.pdf

[18] cipis. 2017. Striped lizard (multi-material) by cipis. https://www.thingiverse.com/thing:2332398

[19] CNC Kitchen. 2023. Recycling Failed 3D Prints with a DIY Filament Extruder: Artme3D. https://www.youtube.com/watch?v=BT04glGDjB4

[20] Jeffrey B. Dahmus and Timothy G. Gutowski. 2007. What gets recycled: an information theory based model for product recycling. *Environmental Science & Technology* 41, 21 (Nov. 2007), 7543–7550. https://doi.org/10.1021/es062254b

[21] Ellen MacArthur Foundation. 2017. A New Textiles Economy: Redesigning fashion's future. https://ellenmacarthurfoundation.org/a-new-textiles-economy

[22] Meltem Eryıldız. 2021. Effect of Build Orientation on Mechanical Behaviour and Build Time of FDM 3D-Printed PLA Parts: An Experimental Investigation. *European Mechanical Science* 5, 3 (Sept. 2021), 116–120. https://doi.org/10.26701/ems.881254

[23] Jeremy Faludi, Natasha Cline-Thomas, and Shardul Agrawala. 2017. The Next Production Revolution, implications for government and business – 3D printing and its environmental implications. 171–213.

[24] Jeremy Faludi, Corrie M. Van Sice, Yuan Shi, Justin Bower, and Owen M.K. Brooks. 2019. Novel materials can radically improve whole-system environmental impacts of additive manufacturing. *Journal of Cleaner Production* 212 (March 2019), 1580–1590. https://doi.org/10.1016/j.jclepro.2018.12.017

[25] Xu Fang, Yunan Qing, Yan Lou, Xin Gao, Hao Wang, Xingyue Wang, Yixuan Li, Yanguo Qin, and Junqi Sun. 2022. Degradable, Recyclable, Water-Resistant, and Eco-Friendly Poly(vinyl alcohol)-Based Supramolecular Plastics. *ACS Materials Letters* 4, 6 (June 2022), 1132–1138. https://doi.org/10.1021/acsmaterialslett.2c00283

[26] FloatingCam. 2023. Old fashion Candy Cane -Twisted / Stranded by FloatingCam | Download free STL model | Printables.com. https://www.printables.com/model/693683-old-fashion-candy-cane-twisted-stranded

[27] Pranav Gharge and Vendel Myles. 2024. Cura: Pause at Height – Simply Explained. https://all3dp.com/2/cura-pause-at-height-how-to-do-it/

[28] Jun Gong, Olivia Seow, Cedric Honnet, Jack Forman, and Stefanie Mueller. 2021. MetaSense: Integrating Sensing Capabilities into Mechanical Metamaterial. In *The 34th Annual ACM Symposium on User Interface Software and Technology (UIST '21)*. Association for Computing Machinery, New York, NY, USA, 1063–1073. https://doi.org/10.1145/3472749.3474806

[29] Vannessa Goodship and J. C. Love. 2002. *Multi-material injection moulding*. Vol. 13. iSmithers Rapra Publishing.

[30] Kishor Kumar Gupta. 2009. Polyvinyl alcohol size recovery and reuse via vacuum flash evaporation. (April 2009). http://hdl.handle.net/1853/28181

[31] Tobias P. Haider, Carolin Völker, Johanna Kramm, Katharina Landfester, and Frederik R. Wurm. 2019. Plastics of the Future? The Impact of Biodegradable Polymers on the Environment and on Society. *Angewandte Chemie International Edition* 58, 1 (2019), 50–62. https://doi.org/10.1002/anie.201805766

[32] Nihed Ben Halima. 2016. Poly(vinyl alcohol): review of its promising applications and insights into biodegradation. *RSC Advances* 6, 46 (April 2016), 39823–39832. https://doi.org/10.1039/C6RA05742J

[33] Paulien Harmsen, Michiel Scheffer, and Harriette Bos. 2021. Textiles for Circular Fashion: The Logic behind Recycling Options. *Sustainability* 13, 17 (Jan. 2021), 9714. https://doi.org/10.3390/su13179714

[34] Owen J. Hildreth, Abdalla R. Nassar, Kevin R. Chasse, and Timothy W. Simpson. 2016. Dissolvable Metal Supports for 3D Direct Metal Printing. *3D Printing and Additive Manufacturing* 3, 2 (June 2016), 90–97. https://doi.org/10.1089/3dp.2016.0013

[35] Jonathan D. Hiller and Hod Lipson. 2009. Fully recyclable multi-material printing. (2009). https://repositories.lib.utexas.edu/items/5038e0ec-d803-498c-b094-4062b3f41674

[36] IARC Working Group on the Evaluation of Carcinogenic Risks toHumans. 1993. d-LIMONENE. In *Some Naturally Occurring Substances: Food Items and Constituents, Heterocyclic Aromatic Amines and Mycotoxins*. International Agency for Research on Cancer. https://www.ncbi.nlm.nih.gov/books/NBK513608/

[37] Alec Jacobson, Daniele Panozzo, and others. 2018. libigl: A simple C++ geometry processing library. https://libigl.github.io/

[38] Aamir Khan Jadoon, Chenming Wu, Yong-Jin Liu, Ying He, and Charlie C.L. Wang. 2018. Interactive Partitioning of 3D Models into Printable Parts. *IEEE Computer Graphics and Applications* 38, 4 (July 2018), 38–53. https://doi.org/10.1109/MCG.2018.042731658

[39] Anketa Jandyal, Ikshita Chaturvedi, Ishika Wazir, Ankush Raina, and Mir Irfan Ul Haq. 2022. 3D printing – A review of processes, materials and applications in industry 4.0. *Sustainable Operations and Computers* 3 (Jan. 2022), 33–42. https://doi.org/10.1016/j.susoc.2021.09.004

[40] Jingchao Jiang, Xun Xu, and Jonathan Stringer. 2018. Support Structures for Additive Manufacturing: A Review. *Journal of Manufacturing and Materials Processing* 2, 4 (Dec. 2018), 64. https://doi.org/10.3390/jmmp2040064

[41] Joshua R. Taylor. 2024. INFORMATION | Recreator3DThe Recreator 3D. https://joshuartaylor.wixsite.com/recreator3d

[42] Jakub Kočí. 2022. Introducing Prusament PETG recycled with calculated life cycle assessment! https://blog.prusa3d.com/introducing-prusament-petg-recycled-with-calculated-life-cycle-assessment_65806/

[43] Nahyun Kwon, Himani Deshpande, Md Kamrul Hasan, Aryabhat Darnal, and Jeeeun Kim. 2021. Multi-ttach: Techniques to Enhance Multi-material Attachments in Low-cost FDM 3D Printing. In *Symposium on Computational Fabrication*. ACM, Virtual Event USA, 1–16. https://doi.org/10.1145/3485114.3485116

[44] Eldy S. Lazaro Vasquez, Mirela Alistar, Laura Devendorf, and Michael L. Rivera. 2024. Desktop Biofibers Spinning: An Open-Source Machine for Exploring Biobased Fibers and Their Application Towards Sustainable Smart Textile Design. In *Proceedings of the CHI Conference on Human Factors in Computing Systems (CHI '24)*. Association for Computing Machinery, New York, NY, USA, 1–18. https://doi.org/10.1145/3613904.3642387

[45] Eldy S. Lazaro Vasquez, Netta Ofer, Shanel Wu, Mary Etta West, Mirela Alistar, and Laura Devendorf. 2022. Exploring Biofoam as a Material for Tangible Interaction. In *Designing Interactive Systems Conference (DIS '22)*. Association for Computing Machinery, New York, NY, USA, 1525–1539. https://doi.org/10.1145/3532106.3533494

[46] Eldy S. Lazaro Vasquez, Hao-Chuan Wang, and Katia Vega. 2020. Introducing the Sustainable Prototyping Life Cycle for Digital Fabrication to Designers. In *Proceedings of the 2020 ACM Designing Interactive Systems Conference (DIS '20)*. Association for Computing Machinery, New York, NY, USA, 1301–1312. https://doi.org/10.1145/3357236.3395510

[47] Lin Lu, Andrei Sharf, Haisen Zhao, Yuan Wei, Qingnan Fan, Xuelin Chen, Yann Savoye, Changhe Tu, Daniel Cohen-Or, and Baoquan Chen. 2014. Build-to-last: strength to weight 3D printed objects. *ACM Trans. Graph.* 33, 4 (July 2014), 97:1–97:10. https://doi.org/10.1145/2601097.2601168

[48] Linjie Luo, Ilya Baran, Szymon Rusinkiewicz, and Wojciech Matusik. 2012. Chopper: partitioning models into 3D-printable parts. *ACM Transactions on Graphics* 31, 6 (Nov. 2012), 129:1–129:9. https://doi.org/10.1145/2366145.2366148

[49] Henrique Teles Maia, Dingzeyu Li, Yuan Yang, and Changxi Zheng. 2019. LayerCode: optical barcodes for 3D printed shapes. *ACM Trans. Graph.* 38, 4 (July 2019), 112:1–112:14. https://doi.org/10.1145/3306346.3322960

[50] I.A. Malik, M. Mirkhalaf, and F. Barthelat. 2017. Bio-inspired "jigsaw"-like interlocking sutures: Modeling, optimization, 3D printing and testing. *Journal of the Mechanics and Physics of Solids* 102 (May 2017), 224–238. https://doi.org/10.1016/j.jmps.2017.03.003

[51] Jonàs Martínez, Jérémie Dumas, and Sylvain Lefebvre. 2016. Procedural voronoi foams for additive manufacturing. *ACM Trans. Graph.* 35, 4 (July 2016), 44:1–44:12. https://doi.org/10.1145/2897824.2925922

[52] W McDonough and M Braungart. 2003. *Cradle to cradle: Remaking the way we make things*. Technical Report.

[53] Vittorio Megaro, Jonas Zehnder, Moritz Bächer, Stelian Coros, Markus Gross, and Bernhard Thomaszewski. 2017. A Computational Design Tool for Compliant Mechanisms. *ACM Trans. Graph.* 36, 4 (2017), 82:1–82:12. https://doi.org/10.1145/3072959.3073636 Publisher: ACM Place: New York, NY, USA.

[54] Anelia Milbrandt, Kamyria Coney, Alex Badgett, and Gregg T. Beckham. 2022. Quantification and evaluation of plastic waste in the United States. *Resources, Conservation and Recycling* 183 (Aug. 2022), 106363. https://doi.org/10.1016/j.resconrec.2022.106363

[55] Eduardo Moreno, Freddys R. Beltrán, Marina P. Arrieta, Gerald Gaspar, Luisa M. Muneta, Ruth Carrasco-Gallego, Susana Yáñez, David Hidalgo-Carvajal, María U. de la Orden, and Joaquín Martínez Urreaga. 2020. Technical Evaluation of Mechanical Recycling of PLA 3D Printing Wastes. *Proceedings* 69, 1 (2020), 19. https://doi.org/10.3390/CGPM2020-07187

[56] Mosaic Manufacturing. 2024. Palette 3 Pro. https://www.mosaicmfg.com/products/palette-3-pro

[57] MosaicManufacturing. 2022. Plant Cell Model (8 Colors) by MosaicManufacturing. https://www.thingiverse.com/thing:5524865

[58] Stefanie Mueller, Tobias Mohr, Kerstin Guenther, Johannes Frohnhofen, and Patrick Baudisch. 2014. faBrickation: fast 3D printing of functional objects by integrating construction kit building blocks. In *Proceedings of the SIGCHI Conference on Human Factors in Computing Systems (CHI '14)*. Association for Computing Machinery, New York, NY, USA, 3827–3834. https://doi.org/10.1145/2556288.2557005

[59] Alessandro Muntoni, Marco Livesu, Riccardo Scateni, Alla Sheffer, and Daniele Panozzo. 2018. Axis-Aligned Height-Field Block Decomposition of 3D Shapes. *ACM Trans. Graph.* 37, 5 (Oct. 2018), 169:1–169:15. https://doi.org/10.1145/3204458

[60] Aamer Nazir, Ozkan Gokcekaya, Kazi Md Masum Billah, Onur Ertugrul, Jingchao Jiang, Jiayu Sun, and Sajjad Hussain. 2023. Multi-material additive manufacturing: A systematic review of design, properties, applications, challenges, and 3D printing of materials and cellular metamaterials. *Materials & Design* 226 (Feb. 2023), 111661. https://doi.org/10.1016/j.matdes.2023.111661

[61] Tuan D. Ngo, Alireza Kashani, Gabriele Imbalzano, Kate T. Q. Nguyen, and David Hui. 2018. Additive manufacturing (3D printing): A review of materials, methods, applications and challenges. *Composites Part B: Engineering* 143 (June 2018), 172–196. https://doi.org/10.1016/j.compositesb.2018.02.012

[62] Nicholas Sharp. 2024. Polyscope. https://polyscope.run/

[63] Martin Nisser, Junyi Zhu, Tianye Chen, Katarina Bulovic, Parinya Punpongsanon, and Stefanie Mueller. 2019. Sequential Support: 3D Printing Dissolvable Support Material for Time-Dependent Mechanisms. In *Proceedings of the Thirteenth International Conference on Tangible, Embedded, and Embodied Interaction*. ACM, Tempe Arizona USA, 669–676. https://doi.org/10.1145/3294109.3295630

[64] Yuta Noma, Koya Narumi, Fuminori Okuya, and Yoshihiro Kawahara. 2020. Pop-up Print: Rapidly 3D Printing Mechanically Reversible Objects in the Folded State. In *Proceedings of the 33rd Annual ACM Symposium on User Interface Software and Technology*. ACM, Virtual Event USA, 58–70. https://doi.org/10.1145/3379337.3415853

[65] Katarzyna Ostapska, Klodian Gradeci, and Petra Ruther. 2021. Design for Disassembly (DfD) in construction industry: a literature mapping and analysis of the existing designs. *Journal of Physics: Conference Series* 2042, 1 (Nov. 2021), 012176. https://doi.org/10.1088/1742-6596/2042/1/012176

[66] Printerior. 2024. 3D Printer Recycling Programs. https://printeriordesigns.com/pages/recycling

[67] Prusa Research. 2024. Original Prusa MMU3 upgrade kit (for MK3S+). https://www.prusa3d.com/product/original-prusa-mmu3-upgrade-kit-for-mk3s-2/

[68] Prusa Research. 2024. PrusaSlicer. https://www.prusa3d.com/page/prusaslicer_424/

[69] Michael L. Rivera, S. Sandra Bae, and Scott E. Hudson. 2023. Designing a Sustainable Material for 3D Printing with Spent Coffee Grounds. In *Proceedings of the 2023 ACM Designing Interactive Systems Conference (DIS '23)*. Association for Computing Machinery, New York, NY, USA, 294–311. https://doi.org/10.1145/3563657.3595983

[70] Robert McNeel & Associates. 2024. Rhinoceros 3D. https://www.rhino3d.com/

[71] Robert McNeel & Associates. 2024. ShrinkWrap. https://www.rhino3d.com/features/shrinkwrap/

[72] Charles Rolsky and Varun Kelkar. 2021. Degradation of Polyvinyl Alcohol in US Wastewater Treatment Plants and Subsequent Nationwide Emission Estimate. *International Journal of Environmental Research and Public Health* 18, 11 (Jan. 2021), 6027. https://doi.org/10.3390/ijerph18116027

[73] Lars Rossing, Rob B. N. Scharff, Bryan Chömpff, Charlie C. L. Wang, and Eugeni L. Doubrovski. 2020. Bonding between silicones and thermoplastics using 3D printed mechanical interlocking. *Materials & Design* 186 (Jan. 2020), 108254. https://doi.org/10.1016/j.matdes.2019.108254

[74] Martin Schmitz, Martin Stitz, Florian Müller, Markus Funk, and Max Mühlhäuser. 2019. ./trilaterate: A Fabrication Pipeline to Design and 3D Print Hover-, Touch-, and Force-Sensitive Objects. In *Proceedings of the 2019 CHI Conference on Human Factors in Computing Systems (CHI '19)*. Association for Computing Machinery, New York, NY, USA, 1–13. https://doi.org/10.1145/3290605.3300684

[75] Christian Schumacher, Bernd Bickel, Jan Rys, Steve Marschner, Chiara Daraio, and Markus Gross. 2015. Microstructures to control elasticity in 3D printing. *ACM Trans. Graph.* 34, 4 (July 2015), 136:1–136:13. https://doi.org/10.1145/2766926

[76] Scott Davidson. 2024. Grasshopper. https://www.grasshopper3d.com/

[77] Silvia Serranti and Giuseppe Bonifazi. 2019. 2 - Techniques for separation of plastic wastes. In *Use of Recycled Plastics in Eco-efficient Concrete*, Fernando Pacheco-Torgal, Jamal Khatib, Francesco Colangelo, and Rabin Tuladhar (Eds.). Woodhead Publishing, 9–37. https://www.sciencedirect.com/science/article/pii/B9780081026762000025

[78] Preeti Sharma, Vittorio Saggiomo, Vincent van der Doef, Marleen Kamperman, and Joshua A. Dijksman. 2021. Hooked on mushrooms: Preparation and mechanics of a bioinspired soft probabilistic fastener. *Biointerphases* 16, 1 (Jan. 2021), 011002. https://doi.org/10.1116/6.0000634

[79] Simplify3D. 2024. Ultimate 3D Printing Material Properties Table. https://www.simplify3d.com/resources/materials-guide/properties-table/

[80] Katherine Wei Song and Eric Paulos. 2023. Vim: Customizable, Decomposable Electrical Energy Storage. In *Proceedings of the 2023 CHI Conference on Human Factors in Computing Systems (CHI '23)*. Association for Computing Machinery, New York, NY, USA, 1–18. https://doi.org/10.1145/3544548.3581110

[81] Peng Song, Zhongqi Fu, Ligang Liu, and Chi-Wing Fu. 2015. Printing 3D objects with interlocking parts. *Computer Aided Geometric Design* 35-36 (May 2015), 137–148. https://doi.org/10.1016/j.cagd.2015.03.020

[82] Lingyun Sun, Deying Pan, Yuyang Zhang, Hongyi Hu, Junzhe Ji, Yue Tao, Shanghua Lou, Boyi Lian, Yitao Fan, Ye Tao, and Guanyun Wang. 2024. Touch-n-Go: Designing and Fabricating Touch Fastening Structures by FDM 3D Printing. In *Proceedings of the CHI Conference on Human Factors in Computing Systems (CHI '24)*. Association for Computing Machinery, New York, NY, USA, 1–14. https://doi.org/10.1145/3613904.3642906

[83] Berrin Tansel. 2017. From electronic consumer products to e-wastes: Global outlook, waste quantities, recycling challenges. *Environment International* 98 (Jan. 2017), 35–45. https://doi.org/10.1016/j.envint.2016.10.002

[84] TerraCycle. 2024. 3D Printing Materials - Zero Waste Box™. https://shop.terracycle.com/en-US/products/3d-printing-materials-zero-waste-box

[85] The CGAL Project. 2024. CGAL 5.6.1 - 3D Alpha Wrapping: User Manual. https://doc.cgal.org/latest/Alpha_wrap_3/index.html

[86] United Nations Environment Programme. 2023. Sustainable production and consumption: Design for disassembly as a circular economy tool - Foresight Brief 031. (2023). https://wedocs.unep.org/20.500.11822/43586

[87] OLEM US EPA. 2016. Fact Sheets on Designing for the Disassembly and Deconstruction of Buildings. https://www.epa.gov/smm/fact-sheets-designing-disassembly-and-deconstruction-buildings

[88] J. Vanek, J. A. Garcia Galicia, B. Benes, R. Měch, N. Carr, O. Stava, and G. S. Miller. 2014. PackMerger: A 3D Print Volume Optimizer. *Computer Graphics Forum* 33, 6 (2014), 322–332. https://doi.org/10.1111/cgf.12353

[89] Joshua Vasquez, Hannah Twigg-Smith, Jasper Tran O'Leary, and Nadya Peek. 2020. Jubilee: An Extensible Machine for Multi-tool Fabrication. In *Proceedings of the 2020 CHI Conference on Human Factors in Computing Systems (CHI '20)*. Association for Computing Machinery, New York, NY, USA, 1–13. https://doi.org/10.1145/3313831.3376425

[90] Pitipong Veerakamolmal and Surendra Gupta. 2000. Chapter 5 - Design for Disassembly, Reuse, and Recycling. In *Green Electronics/Green Bottom Line*, Lee H. Goldberg and Wendy Middleton (Eds.). Butterworth-Heinemann, Woburn, 69–82. https://www.sciencedirect.com/science/article/pii/B9780750699938501590

[91] Kiril Vidimče, Szu-Po Wang, Jonathan Ragan-Kelley, and Wojciech Matusik. 2013. OpenFab: A Programmable Pipeline for Multi-Material Fabrication. *ACM Trans. Graph.* 32, 4 (July 2013). https://doi.org/10.1145/2461912.2461993 Publisher: Association for Computing Machinery Place: New York, NY, USA.

[92] Ludwig Wilhelm Wall, Alec Jacobson, Daniel Vogel, and Oliver Schneider. 2021. Scrappy: Using Scrap Material as Infill to Make Fabrication More Sustainable. In *Proceedings of the 2021 CHI Conference on Human Factors in Computing Systems (CHI '21)*. Association for Computing Machinery, New York, NY, USA, 1–12. https://doi.org/10.1145/3411764.3445187

[93] Shanel Wu and Laura Devendorf. 2020. Unfabricate: Designing Smart Textiles for Disassembly. In *Proceedings of the 2020 CHI Conference on Human Factors in Computing Systems (CHI '20)*. Association for Computing Machinery, New York, NY, USA, 1–14. https://doi.org/10.1145/3313831.3376227

[94] Jiani Zeng, Honghao Deng, Yunyi Zhu, Michael Wessely, Axel Kilian, and Stefanie Mueller. 2021. Lenticular Objects: 3D Printed Objects with Lenticular Lens Surfaces That Can Change their Appearance Depending on the Viewpoint. In *The 34th Annual ACM Symposium on User Interface Software and Technology (UIST '21)*. Association for Computing Machinery, New York, NY, USA, 1184–1196. https://doi.org/10.1145/3472749.3474815

[95] Xiaolong Zhang, Yang Xia, Jiaye Wang, Zhouwang Yang, Changhe Tu, and Wenping Wang. 2015. Medial axis tree—an internal supporting structure for 3D printing. *Computer Aided Geometric Design* 35-36 (May 2015), 149–162. https://doi.org/10.1016/j.cagd.2015.03.012

[96] Peng Zhao, Chengchen Rao, Fu Gu, Nusrat Sharmin, and Jianzhong Fu. 2018. Close-looped recycling of polylactic acid used in 3D printing: An experimental investigation and life cycle assessment. *Journal of Cleaner Production* 197 (Oct. 2018), 1046–1055. https://doi.org/10.1016/j.jclepro.2018.06.275

[97] Caihan Zhu, Tianya Li, Mohamedazeem M. Mohideen, Ping Hu, Ramesh Gupta, Seeram Ramakrishna, and Yong Liu. 2021. Realization of Circular Economy of 3D Printed Plastics: A Review. *Polymers* 13, 5 (Jan. 2021), 744. https://doi.org/10.3390/polym13050744

A Appendix

Algorithm 1: Interface_Generation

Input: a list of input meshes, M_{input}; a scale factor, S; an intersection face reduction ratio, ρ_i; the interface thickness, $t_{interface}$; an interface type, β; a slot count per part, κ; slot face reduction ratio, ρ_s; a slot height, h_{slot}; a slot radius, r_{slot}; mushroom cap height, h_{cap}; mushroom cap radius, r_{cap}

Output: the uncut interface mesh, $M_{uncut\_interface}$; the original input meshes, M_{input}

```
# Perform Pairwise Scaling and Mesh Boolean Intersections
M_reduced ← REDUCE_MESHES(M_input)
P_centroid ← COMPUTE_CENTROIDS(M_reduced)
M_scaled ← UNIFORM_SCALE(M_reduced, P_centroid, S)
M_intersect ← []
foreach m_i ∈ M_reduced do
    foreach m_s ∈ M_scaled do
        if REPRESENTS_SAME_MESH(m_i, m_s) then
            continue
        end
        m_x ← MESH_BOOLEAN_INTERSECT(m_i, m_s)
        M_intersect.PUSH(m_x)                    # Append intersections
    end
end
# Perform ShrinkWrapping and Offsetting
M_uncut_interface ←
  SHRINK_WRAP_OFFSET(M_intersect, t_interface)
# Perform Slot Generation, if needed
if USE_SLOT_JOINTS(β) then
    M_slots ← GENERATE_SLOT_JOINTS(
          M_uncut_interface, β, κ, ρ_s, h_slot, r_slot, h_cap, r_cap)
    M_uncut_interface ← MESH_BOOLEAN_UNION(
          M_uncut_interface, M_slots)
end
return (M_uncut_interface, M_input)
```

Algorithm 2: Interface_Cutting

Input: an uncut interface mesh, $M_{uncut\_interface}$; a list of corresponding input meshes, M_{input}

Output: the cut interface mesh, $M_{cut\_interface}$; a list of the cut input meshes, M_{cut_input}

```
# Perform Mesh Boolean Intersections and Cutting
M_cut_input ← []
M_x_interface ← []
foreach m_i ∈ M_input do
    m_x ← BOOLEAN_INTERSECT(m_i, M_uncut_interface)
    m_cut_i ← BOOLEAN_DIFFERENCE(m_i, m_x)
    M_x_interface.PUSH(m_x)                      # Append intersections
    M_cut_input.PUSH(m_cut_i)                    # Append cut inputs
end
# Perform Boolean Union on Cut Interfaces
M_cut_interface ← BOOLEAN_UNION(M_x_interface)
return (M_cut_interface, M_cut_input)
```

Printing Time			
Name	*Original Object (mins)*	*Object + Interfaces (mins)*	*Increase %*
striped lizard	133	196	47.37
plant cell	123	142	15.45
tongs	143	182	27.27
candy cane	22	33	50.00
hair brush	243	296	21.81
bag holder	254	306	20.47
sheep	252	323	28.17
fidget toy	190	230	21.05
game controller	208	253	21.63

Table 7: Print times for the example objects before and after interfaces are added. All objects are sliced in PrusaSlicer with 0.2 mm layer height and 20% infill. On average an the print time will increase ~28%. However, for objects that have heavily intertwined materials (e.g., the candy cane), print time can increase as much as 50%.

Dissolvable Interface Generation Parameters										
Name	*Scale Factor, S*	*Intersection Face Reduction Ratio, ρ_i*	*$t_{interface}$ (mm)*	*Interface Type, β*	*Slot Count Per Part, κ*	*Slot Face Reduction Ratio, ρ_s*	*h_{slot} (mm)*	*r_{slot} (mm)*	*h_{cap} (mm)*	*r_{cap} (mm)*
striped lizard	1.043	0.0054	1.0	cylindrical	1	0.400	3.0	1.0	–	–
plant cell	1.050	0.0127	1.0	plain	0	–	–	–	–	–
tongs	1.050	1.4706	1.0	cylindrical	1	0.400	3.0	1.0	–	–
candy cane	1.003	0.0848	0.6	plain	0	–	–	–	–	–
hair brush	1.050	0.0548	1.0	cylindrical	3	0.400	3.0	1.0	–	–
bag holder	1.050	0.0691	1.0	mushroom	6	0.001	3.0	1.0	1.5	1.5
sheep	1.050	0.6000	0.8	plain	0	–	–	–	–	–
fidget toy	1.003	1	1.0	plain	0	–	–	–	–	–
game controller	1.003	0.0753	1.0	plain	0	–	–	–	–	–

Table 6: A complete overview of the interface generation parameters used for the example objects.